Design for bird strike crashworthiness using a building block approach applied to the Flying-V aircraft

Sian Ying Chen[a,b], Wydo van de Waerdt[a] and Saullo G. P. Castro[b,*]

[a]Fokker Aerostructures B.V., Edisonstraat 1, 7903 AN Hoogeveen, the Netherlands.
[b]Department of Aerospace Structures and Materials, Delft University of Technology, 2629HS Delft, The Netherlands

ARTICLE INFO

Keywords:
Bird Strike
Crashworthiness
Design
Metallic
Aircraft Design
Flying Wing
Blended wing-body
Flying-V

ABSTRACT

The Flying-V aircraft promises better fuel-burn performance over conventional aircraft, integrating the passenger cabin and cargo volume into the lifting surface. The wing-fuselage and cockpit windows of the Flying-V are exposed to the flight direction, posing a new challenge to the design and certification of structures in terms of bird strike. This study is a first step towards understanding the dynamic load path and contribution of each structural element on the bird strike resistance of the Flying-V leading-edge structures. The goal is to comply with EASAs certification CS-25, while keeping the structure within elastic deformations during a 70 m/s impact with a projectile simulating a 4lb bird. A building block approach (BBA) is proposed for the design for bird strike crashworthiness. At the highest building block level, a sensitivity analysis is performed to identify the effect of each structural element on the plasticity and weight of the leading-edge structures. The trends are used to modify the baseline design and achieve a reduction of 80% of the plastic energy, without any optimization scheme. A critical case of a 133 m/s speed impact of a 4lb bird at 37000 ft cruise altitude shows that there is still penetration in the modified design.

1. Introduction

1.1. Flying-V and the challenge concerning bird strike

In aviation, bird strike regarded as a contact between a moving airborne vehicle and an avian animal. In conventional aircraft, bird strike can cause damage to the aircraft's empennage, wing, windshield, and engine which is a significant threat to flight safety. The critical zone for bird strike of an A350-100 is shown in Figure 1. The Flying-V, a flying wing concept originally developed by Airbus and the Technical University of Berlin [4], promises a large improvement in fuel burn performance compared to conventional competitor aircraft. This design integrates the fuselage hosting the passenger cabin volume into the wing structure, exposes the cabin windows that are now located along the leading edge

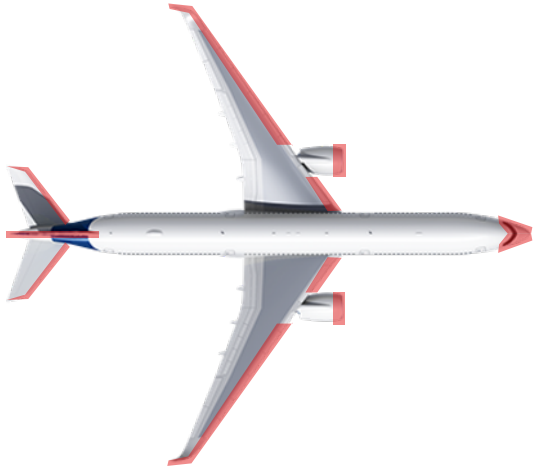

Figure 1: Bird strike critical zone for the A350-1000.

of the aircraft to the flight direction. From the number of reported bird strikes between 2000 to 2014, the wing of a conventional plane has the highest number of reported bird strikes while the impact on the pilot's windshield has the highest injuries and fatalities apart from the engines which are not in the scope of this report [15]. From the reported results [15], it can be deduced that the fuselage of the Flying-

*Corresponding Authors
S.Chen-50@student.tudelft.nl (S. Chen); wydo.vandewaerdt@fokker.com (W. van de Waerdt); S.G.P.Castro@tudelft.nl (S.G.P. Castro)
ORCID(s): 0000-0001-8082-9377 (S. Chen); 0000-0002-1450-9866 (W. van de Waerdt); 0000-0001-9711-0991 (S.G.P. Castro)

V, or the fuselage of similar blended wing body designs, will have the highest probability of bird strike. With the fact that the passenger's cabin windows are now located at the leading edge, it is expected that injuries due to bird strike will increase with the passengers seated next to the windows, contrarily to conventional planes where only the pilots' cockpit windows is under risk of bird strike. Figure 2 illustrates the critical zone of bird strike for the Flying-V.

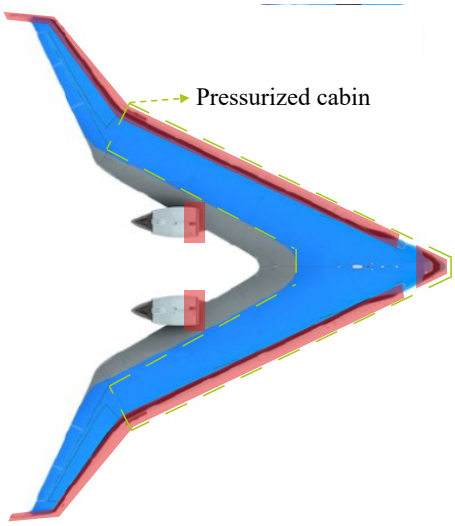

Figure 2: Bird strike critical zone for the Flying-V.

The higher effect of bird strikes on the safety of the Flying-V when compared to conventional planes motivates further development with respect to structural design methodologies for the affected structures, including bird strike considerations that might affect airworthiness already during the preliminary design. In the present study, the cabin windows for the Flying-V are re-examined and re-designed taking as starting point existing structural design and analysis studies [5]. The intended contributions are twofold: achieve a design for the cabin window structures that conforms to the EASA's certification CS-25 for large airplanes; achieve elastic bird strike resistance for the fuselage and window structures under the takeoff and landing speeds of the Flying-V. This report will provide the configuration design of the cabin window and fuselage, their thickness parameters, impact stresses, and energy data.

1.2. EASA certification for bird strike

For convenience, the certification specifications for bird strike from EASA CS-25 Amendment 26 are herein summarized [2]:

- CS 25.631 Bird strike damage: The aircraft must be designed to continue its safe flight and landing when it is struck by a 4lb bird with the flight speed of V_c at sea level or, 0.85 V_c at 2438m (8000ft). The most critical speed should be chosen for the damage tolerance evaluation. Note that V_c is the cruising speed of an aircraft, which is related to flight altitude, aircraft specifications, and aerodynamic parameters.

- CS 25.775 Windshields and windows: Window panes and their supporting structures that are in front of the pilots should not be penetrated by a bird strike impact under the conditions of CS 25.631.

- CS 25.775 Windshields and windows: The aircraft must be designed to minimize the damage of the flying window fragment to the pilots. The window material should not be made of splintering materials. CS 25.775 must be shown for the transparent panes that appear in the front view of the aircraft.

Concerning the bird strike investigation of the Flying-V, the flight speed used for the critical damage location is V_c at sea level. The birds in the weight category of around 4lb are gulls, ospreys, mallards, vultures and similar. High toughness materials such as aluminum alloys and polycarbonate are chosen as the window materials to minimize window fragmentation. Since the passenger windows are all visible from the front view of the aircraft, the passenger windows

are herein treated as the standard pilot's windshield to be compliant with the EASA requirements.

Bird strike physical tests are used to prove that the structure complies with the certification specifications. Wilbeck's team [21] was the first research group that carried physical bird-strike tests on rigid plates. The impact pressure history at the centre of the rigid plate was recorded and theories are generated to predict pressure at different impact speeds and angles. Bird strike experiments are expensive in both costs and time, such that the approach of virtual testing or certification by simulation should be used as much as possible based on validated results that are based on tests carried out by similar structures with sufficiently representative designs and bird strike scenarios [2]. During such validation phase, the worst impact scenarios are identified from the simulation results and the corresponding tests are proposed. After careful validation and the conclusion that the simulation is supported by test data, the design space can be further explored by means of simulations with the goal of achieving a more optimum structural design. The present study is based on numerical models that are build with the intent to identify the critical design scenarios that should be tested in the future.

1.3. Finite Element Approaches for Bird Strike

Different finite element (FE) approaches have been applied on the simulation of the structural behaviour under bird strike conditions. In mesh-based Lagrangian formulation schemes, each mesh node represents a particle that has a fixed connectivity with one or more finite element types. The nodal accelerations are determined according to Newton's second law of motion, where the forces acting on each node are calculated according to connected finite elements, external forces, and according to nonlinear changes of boundary condition, which can be the result of element-to-element contact that develop throughout the dynamic analysis. With the progress of the simulation, the material points that are used to trace the deformation history will following the structural deformation. However, in bird strike simulations, large element distortions and the folding behavior of the distorted elements make the element aspect ratio or skew level unacceptably high, leading to poor numerical conditioning that might create spurious results, or at least creating a very small time step that aborts the simulation process or make the simulation prohibitively expensive. A common measure adopted by the finite element solvers consists of deleting highly distorted elements, whereby the elements that exceed the failure strain are removed and thus disconsidered from further time increments. However, this element removal directly violates the principles of conservation of mass and energy [12]. According to Goyal et al. [9], this loss of mass may result in excessive loss of bird mass due to the fluid behavior of the bird, causing larger-than-expected distortions in the bird model, and reducing the real loads imprinted on the structures being investigated.

Eulerian approaches overcome the element distortion that is intrinsic to Lagrangian formulations, by defining a mesh grid fixed in space that allows the material points to pass through, preventing the element from distortion. However, the Eulerian mesh requires a fine regular or voxelized mesh grid to properly represent complex shapes and complex boundaries to produce accurate results, becoming computationally expensive [6].

Arbitrary Lagrange Eulerian (ALE) methods [3] are a combination of the Lagrangian and Eulerian methods, where the reference coordinate is arbitrary and, depending on the motion, the calculations are Lagrangian-based, with the nodes moving together with the material points, or Eulerian-based, with the nodes fixed and the material points moving through

the mesh. On of the major disadvantages of the ALE method is that the user must specify the optimal mesh motion [8].

Smoothed particles hydrodynamics (SPH) is a mesh-free Lagrangian method in which particles are directly used to represent the material points, without a fixed connectivity as in the case of finite elements. The internal forces are thus calculated not based on connected finite elements, but instead based on the interactions with adjacent particles that fall within the so called smoothing length, which is related to the spherical radial distance in which a particle can influence adjacent particles. Being a Lagrangian method, it keeps some important advantages such as efficient tracking of the material deformations and history-dependent behavior [9]. With the bird behaving like a fluid at high velocity during the event of bird strike, their representation using a cloud or blob of particles within an SPH scheme is advantageous in terms of conservation of mass and energy. The mesh-free behaviour allows the solution involving irregular geometries that produce any free-surface fluidic behaviour, without element distortions or tangling. SPH has also a higher accuracy by following the bird's flow path after impact, which is useful when there are other impacts and interactions with the structure at the vicinity of the first impact location. In the present study, the SPH method is used to simulate the bird whereas FE is used to simulate the Flying-V structures.

1.4. Building Block Approach

The building block approach (BBA) is used as a design methodology for bird strike study on flying wings. The BBA is a way to produce structural data from a process that starts from defining the material coupon, structural element, detailed model, sub-component, full-component to full-aircraft. It is not needed to impact full-aircraft with the bird, a structural component that can represent the affected region by bird strike will suffice. An illustration for the bird strike's BBA of a stabilizer's leading edge and the engine blades is shown in Figure 3 which is created under SAE G-28, Simulants for Impact and Ingestion Testing [17].

From the building block approach, it can be seen that the lowest level consists of coupon testing, where the materials for the structure and bird representation are characterized, and the corresponding numerical models are selected and validated. The material properties for the impacted structure can be determined at this level by using tensile, compression, and lap shear tests. As for the bird representation, it was found that using real bird carcasses for bird strikes has disadvantages such as lack of hygiene and large variations of the bird properties, such as bird density distribution [19, 21]. These variations also depend on the bird species, significantly affecting the impact behaviour of the structures. Therefore, substitute bird materials and geometry were developed on the coupon level to mimic its behaviour while providing a more controlled projectile. Gelatin has been accepted as a material to represent a bird, being considered a superior projectile by most studies [19, 21]. The variables that determine the property of the gelatin bird are chemical formulas, void contents, and reinforced structures [19, 21].

The element level that is the second level of building block approach is used to determine the bird's material behaviour when it is impacted to clamped rigid plates with different scenarios. The impacted plate deforms in the elastic region and acts as a damage indicator whose goal is to show the equivalence between a real bird and an artificial bird impact. The thick plate is made of aerospace-grade aluminum as the standard reference material. Normal and inclined tests are performed to record the impulse reaction. Pressure, force, and strain history are recorded for different bird materials. There are four stages of the pressure history: The initial peak pressure, the pressure decay region,

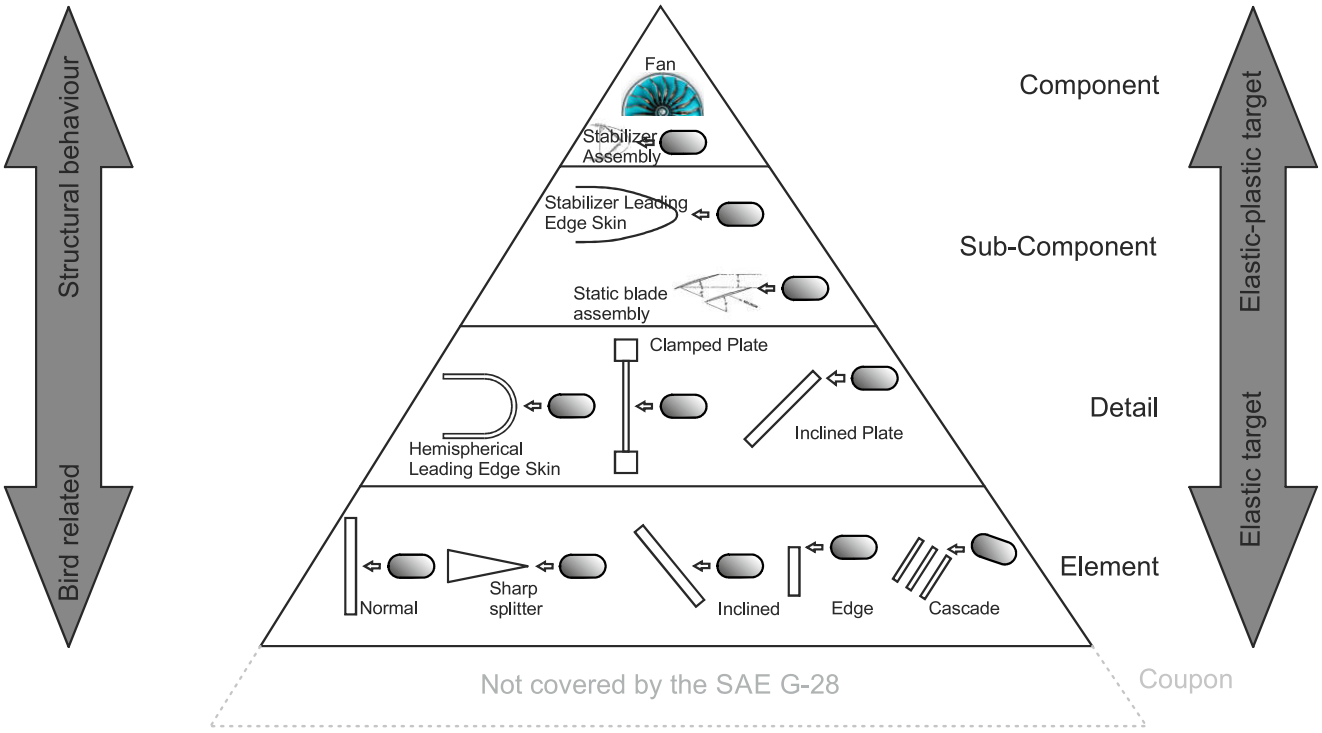

Figure 3: Building block approach for the bird strike investigation. [17]

the steady pressure region and the termination point which represents the end of impact [21]. Split, edge, and cascade impact tests are methods to examine the engine blades' bird strike effect in the case of bird impact with engine structures.

The third level of the building block approach is the detailed level analyses, here the impacted structure is no longer considered as a rigid body, such that its thickness is reduced when compared to the element building block level. Commonly, there is plastic deformation introduced into the model and validation steps, where the impact scenarios still involve simplified geometries. At the fourth level that is the subcomponent assembly, a partial section of the leading edge model is already adopted by the simulations and tests, with the projectile being impacted to the same configuration and thickness of the real structure component, already including some assembly elements such as fasteners, and some representative reinforcements such as stiffeners and ribs. Finally, at the component level, the full assembly of the leading edge or any other impacted structure such as a rotating engine, is impacted by the projectile. Note that at this stage, there is a high maturity in terms of validated modelling capability that covers a broad range of geometries and impact scenarios.

2. Methodology

2.1. Building block approach of the Flying-V

Figure 4 shows the proposed building block approach (BBA) for the bird strike assessment of the Flying-V wing-fuselage leading edge windows. Ideally, the simulations performed on each level and herein demonstrated should be supported by physical tests. However, in this study that is part of the preliminary design of the Flying-V aircraft, only the simulations at the coupon level are supported by tests. Thus, at the coupon level, the properties of aluminum alloy 7050-T7451, cladded aluminum 2024-T42, bird material, and polycarbonate sheets are defined in the simulation model and validated by means of physical tests and literature.

At the element level, the normal and inclined impact of the bird is performed on a 100mm thick polycarbonate and

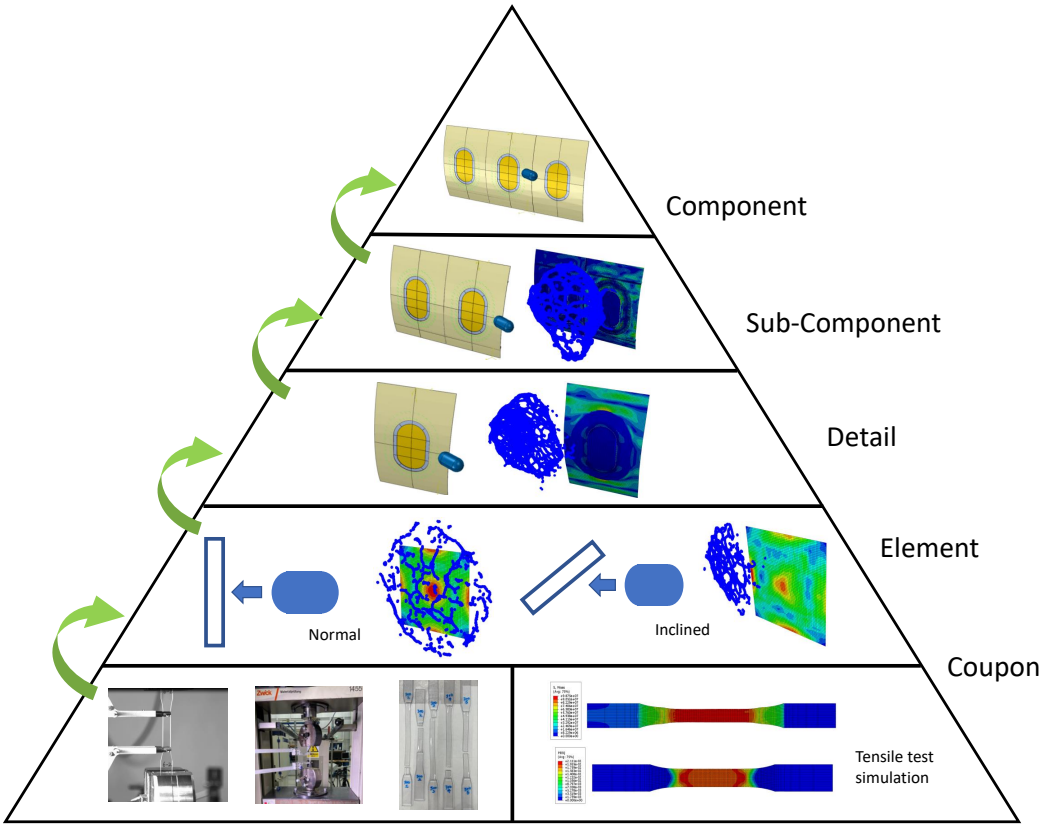

Figure 4: Bird strike BBA road-map for the Flying-V.

aluminum 2024-T42 plates with speeds of 70m/s and 200 m/s. The pressure-time history at the plate centre location is recorded and presented. The element level is used to compare a real bird impact against a user-defined bird.

On the detailed level, one window section is impacted by a 4lb bird with a speed of 70 m/s. The distribution and the values of the stress and plastic strain are examined throughout the impact history. The structural components are simplified and fixated by tie constraints using the Simulia Abaqus software. On the sub-component level, two window sections are presented. Fuselage frames, stringers, the whole window configuration, and fasteners are added on this level to perform a more rigorous bird strike investigation. Multiple locations on the fuselage frame and the window structure are impacted to search for the critical location that generates the maximum plastic energy. The thicknesses of the window structure components are adjusted in a sensitivity analysis to find out which component can contribute the highest decrease in plasticity. Furthermore, the 4lb bird with the cruising speed at 37000ft (highest flight altitude ever recorded for a bird strike) is impacted on the critical location of the window. The feasibility of this research's two goals can be answered at the sub-component level. Simulations performed at the component level with three window sections are left for future work, when more information about the Flying-V geometry and design will be available. The Flying-V's window structure should be tested with bird strike on the component level aiming validation of the simulation models. After that, more simulations could be done by impacting at different locations, different bird masses, and different impact speeds. At such level of validated modelling, the simulation results could be used to support the Flying-V certification

Aluminum Alloy	7050-T7451	7075-T7351	Alclad-2024-T42
Density (kg/m^3)	2800	2800	2770
Elastic Modulus (MPa)	71000	71000	68300
Poisson Ratio	0.33	0.33	0.33
Fracture Strain	0.08	0.07	0.2
Fracture Energy (J/m^2)	110000	110000	130000
Softening Behaviour	Exponential	Exponential	Exponential

Table 1
Material properties of the aluminum alloys used in the wing-fuselage and window frame structures.

campaign.

2.2. Material properties

The aluminum alloys' properties that are applied to the Flying-V wing-fuselage and window structure, and the material data from the fasteners, are obtained from Fokker Aerostructure's material database. The Polycarbonate material properties used for the passenger window pane are obtained from experiments, and the bird material data, represented as gelatin, is obtained from literature. This sub-section is dedicated to detail all the aforementioned material properties.

2.2.1. Aluminum alloys for the wing-fuselage and window structures

Table 1 provides the material properties for the aluminum alloys 7050-T7451, 7075-T7351, and cladded aluminum 2024-T42. The actual values for the fracture strain and fracture energy, obtained from Fokker Aerostructure's material database, are not provided due to confidential reasons, and the values herein published are representative and rounded up to the second digit after the decimal point for the fracture strain; and to the fifth digit for the fracture energy.

In Table 1, ductile damage behaviour of aluminum alloys contains the fracture strain and fracture energy. Ductile damage in Abaqus is initiated after the true stress reaches the yield stress of the material with a zero plastic strain. After the alloys are loaded beyond the ductile damage initiation point, the softening of the yield stress and the degradation of the elastic modulus starts to progress until the effective load carrying capacity reaches zero. The corresponding point where the load reaches zero and the material fractures is defined as the failure strain or the fracture strain shown in Table 1. If element deletion is activated for the model, which is an available resource in Abaqus, the element is deleted at the fracture strain point. The stress-strain curves of the three aluminum alloys can be found in the Metallic Materials Properties Development and Standardization (MMPDS) handbook [1], which are equivalent to the actual properties used in this project. The fracture toughness (K_{IC}) are indicated for the three alloys which can be calculated into fracture energy (G_{IC}) using:

$$G_{\mathrm{IC}} = \left(1 - \nu^2\right) K_{\mathrm{IC}}^2 / E \tag{1}$$

where: E given in $[MPa]$, and ν, are respectively the elastic modulus and the Poisson ratio of the material; K_{IC} given in $[MPa\sqrt{m}]$ is the fracture toughness which can be measured by using compact tension (CT) coupons tests. In Abaqus, using the fracture toughness (G_f) as a damage evolution parameter creates a stress-displacement response after the softening initiation, rather than a stress-strain response. This is an advantage since during softening, the stress-strain response cannot accurately present the material's behaviour due to its dependency on the mesh size.

The stress-strain curves are also provided as figures in which data points can be extracted and transformed into true

stress-strain curves. Comparing the three alloys in Table 1 and using the MMPDS handbook, the cladded aluminum 2024-T42 has the highest fracture toughness. Aluminum 7075-T7351 and 7050-T7451 have a higher tensile strength than 2024, but a lower fracture toughness. They have similar elastic properties and 7050-T7451 has higher toughness and higher tensile stress. Therefore, the two aluminum alloys that are used in the model are aluminum 2024-T42 and 7050-T7451.

2.2.2. Gelatin material used for the bird representation

To define the bird gelatin material in Abaqus using Smoothed Particle Dynamics (SPH), one needs to define the density and an equation of state (EOS) that relates the density with the isostatic pressure. Although birds have different shapes among different species, the density of all the birds is close to 950 kg/m^3, and this value is customarily considered uniform throughout the bird [16]. The main content of the bird is water and during impact, its viscosity and strength can be neglected. Therefore, the bird behaves like a fluid during impact which gives a hydrodynamic response to the structure. Regarding the EOS, the $U_s - U_p$ is adopted in Abaqus/Explicit, which describes a linear relation between the shock velocity U_s, and the particle velocity U_p. The $U_s - U_p$ method in Abaqus defines a pressure for materials in compression as Equation 2:

$$p = \frac{\rho_0 c_0^2 \eta}{(1 - s\eta)^2}\left(1 - \frac{\Gamma_0 \eta}{2}\right) + \Gamma_0 \rho_0 E_m \tag{2}$$

where: ρ_0 is the reference density when the medium has no pressure; η is the nominal volumetric compressive strain $1 - \rho_0/\rho$; ρ is the current density that varies during the impact time; Γ_0 is a material constant; E_m is the internal energy per unit mass; s is a constant that defines the linear $U_s - U_p$ slope; and c_0 is the speed of sound in the medium. The properties of the bird that are used in Abaqus are shown in Table 2. The data is based on the Mie-Grüneisen EOSs parameters for water [16, 20].

Properties	Value
$\rho_0(kg/m^3)$	950
$c_0(m/s)$	1480
s	0.92
Γ_0	0.1

Table 2
Gelatin material properties used in Abaqus for the bird representation.

2.2.3. Polycarbonate material for the window pane

The polycarbonate material from Arla Plast MAKROCLEAR is used for the window pane. The stretched polycarbonate sheets have 10 times the impact strength of a high-impact PMMA, and similar density. The density and the fracture energy used for the polycarbonate material properties in Abaqus come from a datasheet [14]. The elastic, plastic and ductile damage properties; are determined by tensile testing, as described next.

Polycarbonate is a strain rate-dependent material for which the properties for low strain rates can be obtained according to the ASTM D638 standard test method for the tensile properties of plastics, which is a quasi-static tensile test that is applicable only to strain rates less than 0.25 s^{-1}. However, high-speed bird strike impact requires the use of material properties that correspond to strain rates of the order of thousands strain units per second. Fu et al. [7] performed dynamic tensile tests at high strain rates by using a split Hopkinson tension bar (SHTB) system that is shown in Figure 5. The results showed that the polycarbonate material has an elastic and plastic behaviour stage, and that the yield stress is sensitive to the strain rate. When the strain rate increases, the yield stress increases while the failure strain decreases. The Young's modulus is independent or varies little with dif-

ferent strain rates.

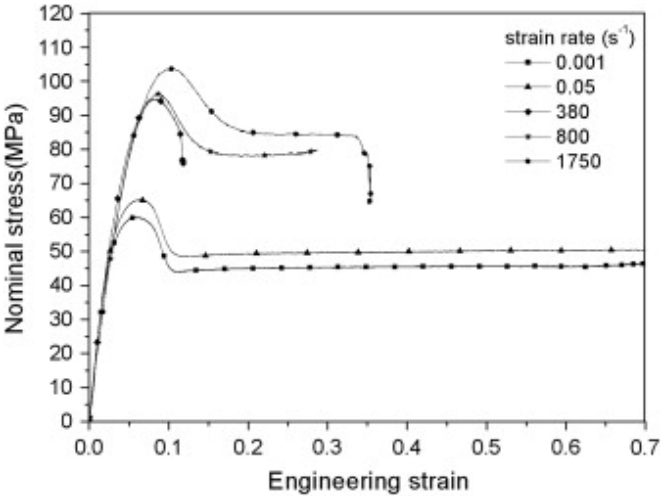

Figure 5: Tensile stress-strain curves at different strain rates [7]

The tensile testing of the polycarbonate is performed according to the ASTM D638 standard test method. The dimensions for a type-I polycarbonate coupon with a thickness of 5 mm is shown in Figure 6.

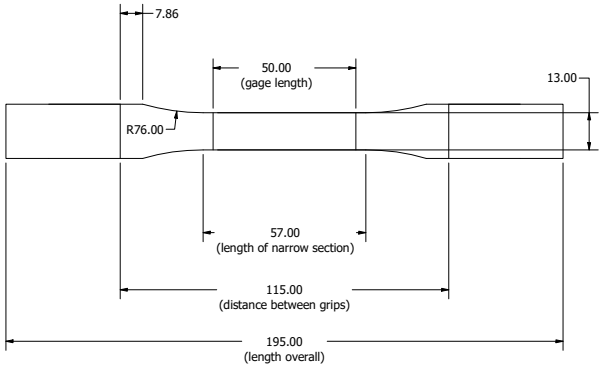

Figure 6: Polycarbonate coupon dimensions (in mm).

The tensile test plan is presented in Table 3.

According to the ASTM D638, each loading rate needs to be tested with five coupons, which is performed with the ZwickRoell machine but not for the MTS machine since the high loading rates are not within the range of the standard. An extensometer is applied to measure the displacement of the 6 s^{-1} loading rate coupons starting from the initial gauge length. The tensile strain rate is limited up to 3 s^{-1}, which is still not high enough to present the polycarbonate behaviour at high impact speeds. Therefore, stress-strain properties for high strain rates that are more compatible with the bird strike impact are determined based on the results from Fu et al. [7]. The cross-section dimensions of the narrow coupon sections are measured before the test, and later used for determining the engineering stress. Force and nominal strain data are recorded during testing. To plot the nominal stress-strain curve, the force data is divided by the unloaded cross-section of each coupon. The nominal strain data are computed by the displacement of the grip divided by the grip length shown in Figure 6. The true stress and true strain are calculated to determine the level of plasticity using Equation 3. The plastic strain ε^p is then computed by Equation 4; where ε^t is the total strain that equals the true strain ε.

Testing Machine	Loading Rate (mm/min)	Strain Rate (%)	Number of Coupons
ZwickRoell 20 kN	6	0.0009	5
ZwickRoell 20 kN	300	0.0432	5
ZwickRoell 20 kN	750	0.1058	5
MTS 15kN	7500	1.0897	2
MTS 15kN	15000	2.2015	2
MTS 15kN	30000	3.1207	2

Table 3
Tensile test planning.

$$\varepsilon = \ln\left(1+\varepsilon_{\text{nom}}\right)\ \sigma = \sigma_{\text{nom}}\ \left(1+\varepsilon_{\text{nom}}\right) \tag{3}$$

$$\varepsilon^{pl} = \varepsilon^{t} - \frac{\sigma}{E} \tag{4}$$

A coupon model is constructed in Abaqus to numerically validate the tensile test using the experimentally determined material properties. A nominal stress-strain curve is generated from the simulation and compared with the testing re-

Analysis Type	Dynamic Explicit
Geometric Order	Linear
Element Type	Hexahedron C3D8R
Element Number	11040
Reduced Integration	On
Element Deletion	On
Max Degradation	0.85

Table 4
Polycarbonate coupon, finite element data.

sults. A dynamic, explicit analysis is performed using solid C3D8R elements, with the element type and corresponding data shown in Table 4. For the boundary conditions, the first clamping end is set as encastered, while at the second clamping end the displacements are only allowed in the loading direction. A prescribed displacement of 100mm is assigned to a centre reference point at the second clamping end, and the reaction load is measured at each time step. The nominal stress-strain curve is generated by the reaction force and displacement history of the displacement reference point. The nominal stress-strain are determined by diving the reaction force to the narrow section mean cross-section, and dividing the displacement by the grip length in Figure 6.

2.3. Impact scenarios

According to the FAA database from 2000-2014 [15], 70 % of the bird strikes occurred at an altitude below 500 feet (152.4 meters). Aircraft at heights between 0 to 100 feet (30.48 meters) constitute more than 60 % of registered aircraft destruction. Among the bird strike cases that were recorded during flight [15], over 90 % of the cases occurred during the approach, landing roll, take-off run and climb. According to the high probability of the bird strike at aircraft height and flight phases, the impact velocity studied in this project is the approach and take-off speed of the Flying-V.

To calculate the cruise speed at different altitudes, parameters of the Flying-V are provided shown in Table 5 [13].

MTOW (kg)	$266(10^3)$
b (m)	65
S (m^2)	886.66
$C_{D,0}$ (Counts)	54.3
Lift-to-drag-ratio	21.7
e	0.811
$\rho_{air,0}$ (kg/m^3)	1.25
$\rho_{air,8000}$ (kg/m^3)	0.9638
$\rho_{air,37000}$ (kg/m^3)	0.36976
AR (m)	4.7651
f_{carson}	1.32
Sweep Angle	63.5°

Table 5
Flying-V parameters

Three cruise speeds are calculated, at sea level, 8000 feet (2438.4 meters), and 37000 feet (11277.6 meters). Sea level and 8000 feet altitudes are calculated by the EASA requirements. The 37000 feet altitude is the highest altitude ever recorded for a bird strike.

The lift coefficient of the wing is calculated by Equation 5:

$$C_{L,altitude} = \frac{MTOW}{\frac{1}{2}\rho_{air,altitude} V_{c,altitude}^2 S} \tag{5}$$

Using $C_{L,altitude}$, the drag coefficient $C_{D,altitude}$ can be calculated by Equation 6,

$$C_{D,altitude} = C_{D,0} + \frac{C_{L,altitude}^2}{\pi e AR} \tag{6}$$

where $C_{D,0}$ is presented in counts, one counts is 0.0001.Therefore the value of $C_{D,0} = 0.0054$. After obtaining the lift and drag coefficient, using the lift and drag ratio the cruising speed $V_{c,altitude}$ can be calculated using the relation in Equation 7.

$$\frac{C_{L,altitude}}{C_{D,altitude}} = 21.7 \tag{7}$$

The cruising speed of the three altitudes are shown in

$$\begin{aligned} V_{c,0} &= 71.126(m/s) \\ V_{c,8000} &= 80.228(m/s) \\ V_{c,37000} &= 133.38(m/s) \end{aligned} \tag{8}$$

According to EASA regulations, $V_{c,8000}$ times 0.8 is lower than $V_{c,0}$, which is less critical. Thus, the bird strike velocity that is applied in the present simulation is approximated as 70 m/s.

2.4. Bird strike simulation in the building block approach

2.4.1. Element level

The element level contains the bird model and the thick plate model. For the bird's geometry, various geometries such as ellipsoid, hemispherical-ended cylinder, straight-ended cylinder and sphere are proposed. The comparison of pressure history between different geometries with the experiment is shown in Figure 7. It can be seen that the straight-ended cylinder has the highest pressure and the hemispherical-ended cylinder had the closest Hugoniot pressure compared to the experiment test, although it is still four times higher. Despite this, the hemispherical-ended cylinder geometry is still the most common geometry used to represent bird strike, and therefore it is the chosen representation for the bird geometry.

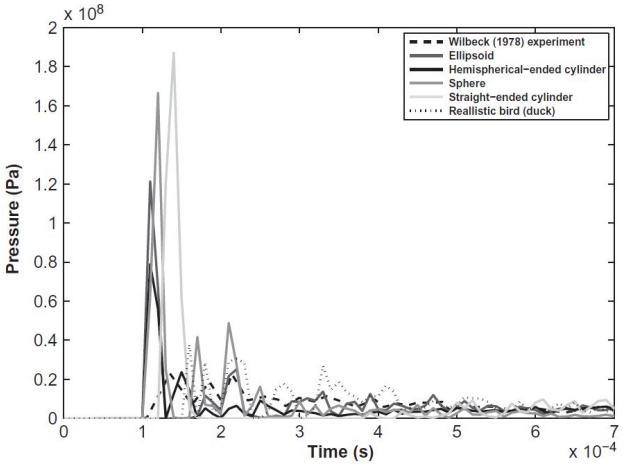

Figure 7: Centre impact pressure history of the four geometries.[16]

Using R, the bird model is constructed shown in Figure 8.

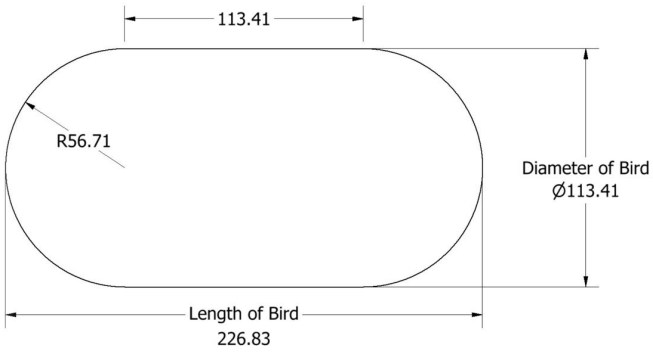

Figure 8: 4lb bird model dimensions (mm)

For the hemispherical-ended cylinder, the length-to-diameter ratio is set to be two [16]. With a bird mass of 4 lb (1.814 kg) and density of 950 kg/m^2, the volume can be calculated as 1.91×10^{-3} m^3. The radius of the hemispherical-ended cylinder R_{bird} can be determined from:

$$\begin{aligned} \tfrac{4}{3}\pi R_{bird}^3 + 2\pi R_{bird}^3 &= 1.91e-3 \\ R_{bird} &= 0.0567(m) \end{aligned} \tag{9}$$

The bird geometry is first approximated using hexahedral C3D8R Lagrangian finite elements, which are then converted to SPH particles by using a time-based criterion. A time threshold of 0 (zero) is specified to convert all the parent elements to particles at the beginning of the impact event. The PPD (particles per isoparametric direction) is set as 1 (one) by default. The bird's mesh and its conversion to particles is illustrated in Figure 9.

For the plate model, aluminum 2024-T42 is assumed for the fuselage skin, and polycarbonate material for the pane. The geometry consists of a one-meter by one-meter square deformable shell with a thickness of 100 mm. The bound-

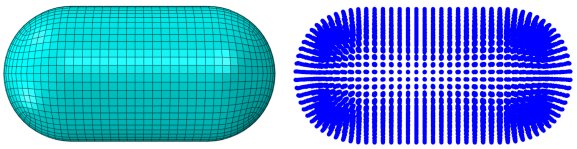

Figure 9: Bird's model conversion to particles by SPH method

Analysis	1	2	3	4	5	6	7	8
Polycarbonate	v	v	v	v				
Al 2024-T42					v	v	v	v
Inclined	v	v			v	v		
Normal			v	v			v	v
70 m/s	v		v		v		v	
200 m/s		v		v		v		v

Table 6
Element level analysis plan

ary conditions are clamped at the four edges. In the Abaqus software, element deletion for the plates is activated. Two speeds which are 70 m/s and 200 m/s are tested for impact. The normal impact of the plate and a plate inclination of 63.5 degrees with respect to the impact direction is performed, which corresponds to the sweep angle of the Flying-V leading edge. The simulation planning is given in Table 6.

The model set up table is shown in Table 7. The normal and inclined impact model assemble are shown in Figure 10.

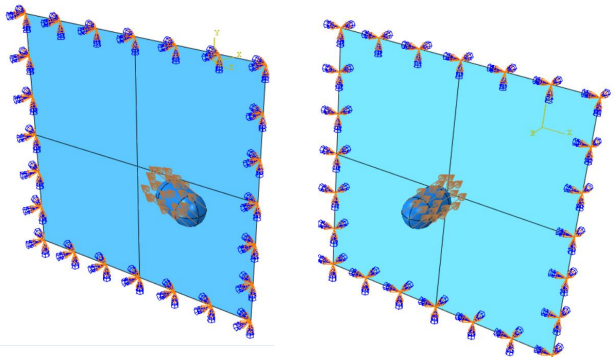

Figure 10: Element level, inclined and normal impact load and boundary conditions

Model	Bird	Plate
Shell Thickness (mm)	- -	100
Material	- Gelatin	- Aluminum 2024-T42 - Polycarbonate
Mesh element Type	- Explicit, Linear - C3D8R - Conversion to Particles: On - Time based criterion - Time threshold: 0	- Explicit, Linear - S4R - Reduced integration: Off - Element Deletion: On
Element Global Size (m)	0.0065	0.015

Table 7
Element level model information

2.4.2. Detail level

The window design is modified from the patented passenger window from Mitsubishi Aircraft Corporation as a reference. The patented window design is shown in Figure 11 [10].

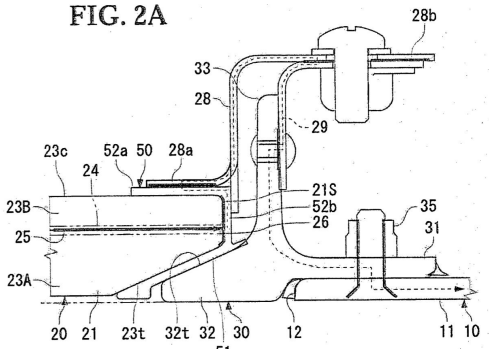

Figure 11: Mitsubishi Aircraft Corporation passenger window design patent.[10]

For the window design at the detailed level, a simplified representation based on three components is proposed: one layer of polycarbonate pane; a window frame; and a fuselage skin. The rubber gasket seal and fillets are ignored, and the fasteners are simplified as tie constraints. The skin is set to be 2.5mm thick and the rest of the window component cross-sections are traced based on the full-scale dimensions provided by Mitsubishi Aircraft Corporation [10]. The tapered window frame geometry is simplified as a flat surface, and

Model	Bird	Window Frame	Window Pane	Fuselage Skin
Shell Thickness (mm)	–	3	9.6	2.5
Material	Gelatin	Al 7050-T7451	Polycarbonate	Al 2024-T42
Mesh element Type	- Explicit, Linear - C3D8R - Conversion to Particles: On - Time based criterion - Time threshold: 0	- Explicit, Linear - S4R - Reduced Integration: On - Element Deletion: On	- Explicit, Linear - S4R - Reduced Integration: On - Element Deletion: On	- Explicit, Linear - S4R - Reduced Integration: On - Element Deletion: On
Element Global Size (m)	0.004	0.0045	0.005	0.007

Table 8
Detail level model passenger window information

the thicknesses of the components are homogeneous. The fuselage skin section has a frame pitch of 635 mm with a leading-edge cylindrical curvature of 1.25m. The model is shown in Figure 12 with a window size of horizontal width 0.244 m and vertical height of 0.44m (0.244mx0.44m).

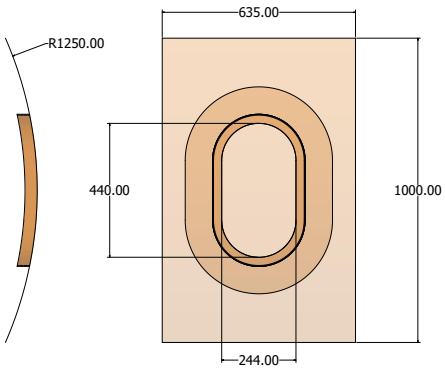

Figure 12: Detailed level window drawing design dimensions in mm

For comparative reasons, the authors created models representing the Airbus A350 and Boing 787 windows. No reliable dimensions of the Airbus A350 and the Boeing 787 passenger windows were found in the literature, requiring assumed approximated dimensions based on pictures of these airplanes: 0.242 m×0.34 m for the Airbus A350; and 0.272 m× 0.47 m for the Boeing 787. The window models are also created in Abaqus, as shown in Table 8. Shell elements of type S4R are used, with 4-nodes with reduced integration.

The meshed model, rear model view and the the boundary conditions are shown in Figure 13. The top and bottom edges of the fuselage skin are clamped and the sides edges are defined as symmetric. A velocity of 70 m/s is assigned to the bird model.

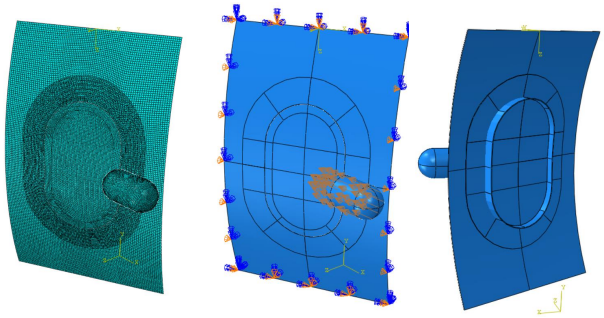

Figure 13: Detailed Level, meshed model and boundary conditions.

2.4.3. Sub-component Level

Two window sections are used in the sub-component level. The model is expanded from the detailed model by adding pane clamp, clamp fastener, stringers, fuselage frames and point-based fasteners. The model information is shown in Table 9.

Reduced integration is turned off at this level to generate more accurate results. The model of the fuselage frame and stringers is traced from the configuration of the Convair 880 [11]. The exploded view of the sub-component is shown in Figure 14.

Tie constraints are used to combine the two fuselage skin,

Model	Shell Thickness	Material	Mesh element Type	Element Global Size (m)
Bird	–	Gelatin	Explicit, Linear C3D8R Conversion to Particles: On Time based criterion Time threshold: 0	0.0045
Window Frame	3mm	Al 7050-T7451		0.006
Window Pane	9.6mm	Polycarbonate		0.0055
Fuselage Skin	2.5mm	Al 2024-T42	Dynamic explicit	0.0065
Pane Clamp	3mm	Al 7050-T7451	Linear	0.0055
Clamp Fastener	2mm	Al 7050-T7451	S4R	0.005
Stringer	2.5mm	Al 2024-T42	Reduced integration: Off	0.025
Fuselage Frame	2.5mm	Al 2024-T42	Element Deletion: On	0.01
Fuselage Shear Clips	2.5mm	Al 2024-T42		0.005

Table 9
Sub-component level passenger window model information

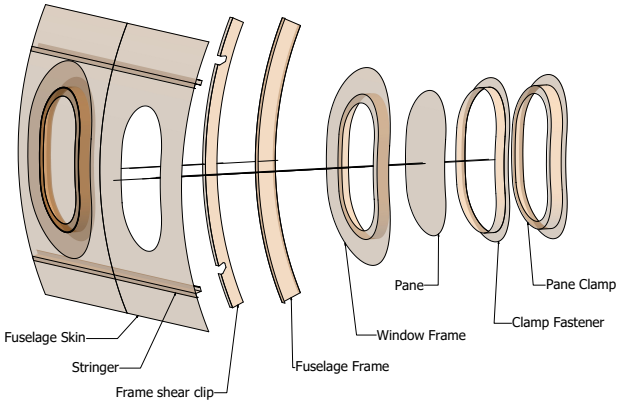

Figure 14: Sub-component level surface model exploded view.

	Metal (m)
Edge distance	0.02
Pitch	0.04
Fastener spacing	0.05

Table 10
Point based fastener distance in Abaqus model.

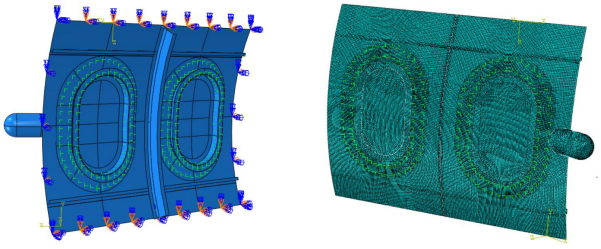

Figure 15: Sub-component, meshed model and boundary conditions.

stringers to the skin, frame clips to the skin and frame to the frame clips. The passenger window structure components are attached by point-based fasteners with 10 mm in diameter, as illustrated in Figure 11. The skin and window frame are attached by double rowed fasteners to allow a stiffer bonding between the impacted structure. The fastener mounting parameters are shown in Table 10 by applying guidelines provided by Fokker Aerostructures. The model constructed in Abaqus is shown in Figure 15. The boundary conditions are identical to the detailed model. The bird impact velocity remains at 70 m/s with an impact angle of 63.5 degrees, to represent the Flying-V sweep angle of the leading edge.

Critical locations of the bird strike on the Flying-V fuselage and passenger window are determined at this level. The goal is to determine the impact location that generates the highest amount of plastic deformation, measured by the amount of plastic energy absorbed by the structures during the bird strike. With the critical region for plastic deformation determined, it is possible to facilitate the design of structures that would prevent the structure from achieving plastic deformation. The skin at the fuselage frame shear clip and the passenger window are the two critical impact locations herein studied. Since the model is symmetric along the horizontal centre line, the impact points above the centre line can represent the impact behaviours described below. Three im-

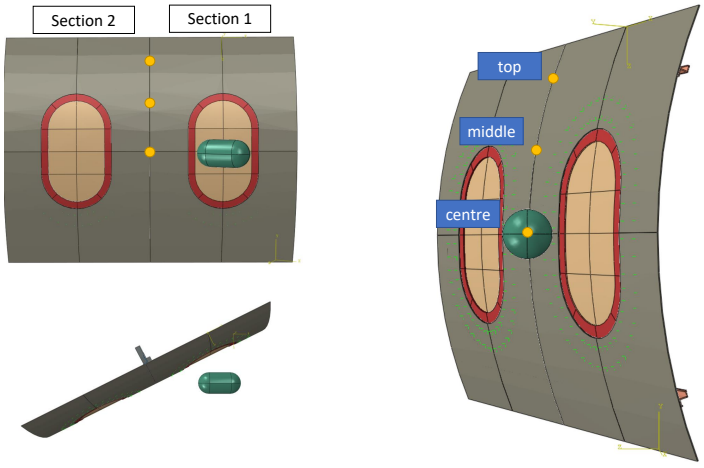

Figure 16: Fuselage frame 3 impact location study.

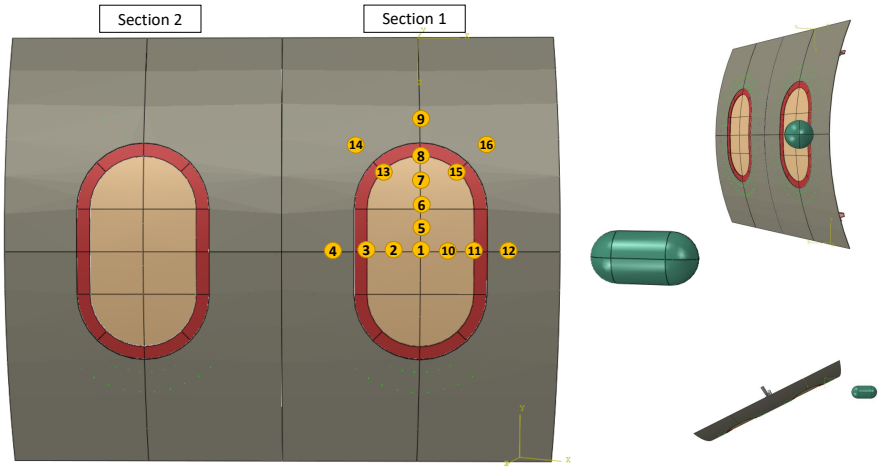

Figure 17: Passenger window 16 impact location study.

pact locations are planned for the fuselage frame impact, as depicted in Figure 16.

For the window, 16 impact locations are planned, as shown in Figure 17.

Impact locations 3, 8, 11, 13, 15 are the pane and window frame boundaries. Impact locations 4, 9, 12, 14, 16 are the fuselage skin section stiffened by the window frame behind them.

3. Results and discussion

3.1. Polycarbonate Material Characterization

The nominal and true stress-strain data of different loading rates are compared by selecting the first specimen of the same loading rate samples shown in Figure 18. Figure 18 shows that the yield stress and the material toughness are increasing as the loading rate increases, which is in good agreement with the literature results from Fu et al., shown in Figure 5.

The maximum tensile strength (nominal) determined from

Loading Rate (mm/min)	6	300	750	7500	15000	30000
Mean Tensile Strength at Yield (MPa)	64.146	68.728	69.924	74.303	76.459	76.945

Table 11
Experimental mean tensile strength at yield

Loading Rate (mm/min)	6	300	750	7500	15000	30000
Mean Nominal Failure Strain (%)	87.6177	76.4842	72.2048	64.1896	66.0747	75.8940

Table 12
Experimental mean nominal failure strain

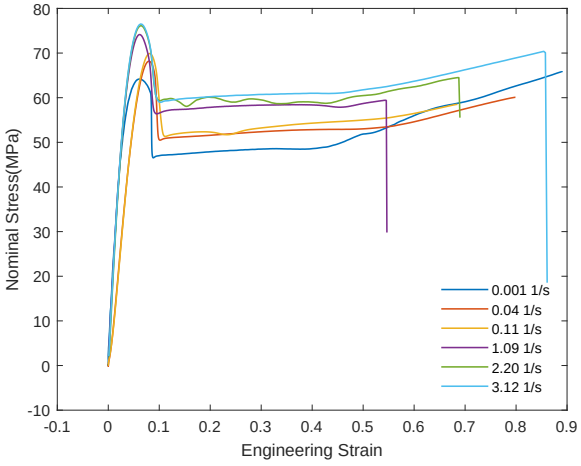

Figure 18: Experimental nominal stress-strain curves for different loading rates

Figure 18 is defined as the maximum stress that is sustained during the tensile test. The mean maximum tensile strength for each loading rate are shown in Table 11.

The nominal failure strain determined from Figure 18 is defined as the strain at the rupture point. The mean values for each loading rate are shown in Table 12.

The strain rate is determined by performing a first-order polynomial fit of the strain-time data point generated by the data logging. The slope is defined as strain rate. The mean values of the strain rates for the corresponding loading rates are shown in Table 13.

Young's modulus is determined by performing a first-order polynomial fit of a range of stress-strain data points. Since the norm ASTM D638 did not specify a range, standards from ISO 527 (Plastics Determination of tensile properties) are used for reference. The range of the data is defined as the strain interval between 0,05 % and 0,25 %. Only the 6 mm/min loading rate is used to determine the Young's modulus, since the extensometer can only be attached to low loading rates. The Young's modulus of the 5 specimens and the mean value at a loading rate of 6 mm/min is shown in Table 14.

The true stress-strain curves are shown in Figure 19. The

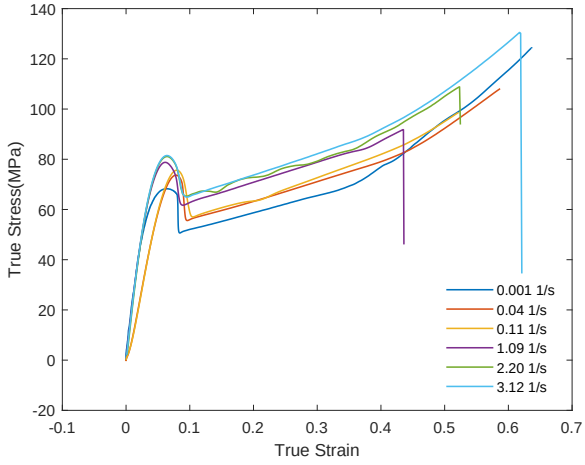

Figure 19: Experimental true stress-strain curve for different loading rates

first plasticity data point of each strain rate in Abaqus has to start with a plastic strain of 0, the corresponding true stress is the true yield stress. It is defined in ISO 527 at the data point that the tangent slope in the true stress-strain curve equals zero. To simplify this, the maximum true stress at the elastic-plastic transfer true strain range is determined for the stress of zero plastic strain. The true yield stress and its corresponding true strain are given in Table 15.

The comparison of simulation with testings is shown in

Loading Rate (mm/min)	6	300	750	7500	15000	30000
Strain Rate (%)	0.0009	0.0432	0.1058	1.0897	2.2015	3.1207

Table 13
The corresponding mean strain rate of the loading rates

Specimen Number	1	2	3	4	5	mean
Young's Modulus (GPa)	2.0389	2.1257	2.1462	2.9143	1.6321	2.1714

Table 14
Young's modulus and the mean value for 6 mm/min loading rate.

Figure 20. Young's modulus for the simulation is 2.635 GPa,

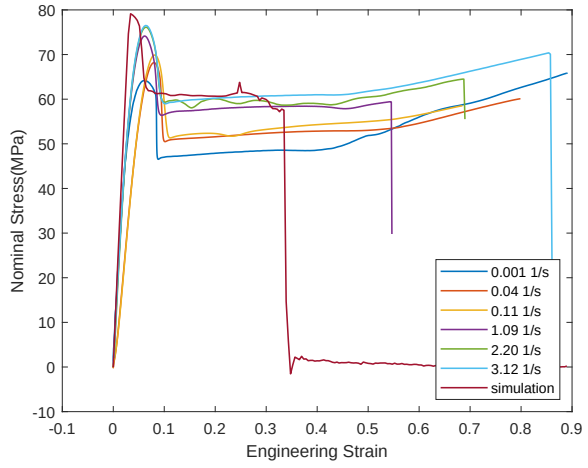

Figure 20: Experimental nominal stress-strain compared with Abaqus dynamic explicit simulation.

higher than all the modulus determined for testing. However, this value matches the range given in the manufacturer datasheet which is >2300 MPa. The result of the simulation conforms better with the higher strains rate 2.2 and 3.12 s^{-1}. The tensile testing is recorded with a camera for loading rates of 6, 300, 750 mm/min and a high-speed camera for 7500, 15000, 30000 mm/min. An example of the tensile test history is shown in Figure 21 using loading rate 300mm/min coupon 5 as an example. The Mises stress and the equivalent plastic strain (PEEQ) history is shown in Figure 22.

It is observed that necking can start to occur at one or two locations simultaneously shown in Figure 23 (a) at loading rate 7500 mm/min specimen 1. For a fracture at a higher tensile loading rate of 30000 mm/min, the reaction stresses that are generated upon fracture propagate back to the specimen causing the wave-like deformation shown in Figure 23 (b).

A clear discrepancy between the simulation and the testing result is the strain at failure, resulting in a toughness difference. In Abaqus, an energy type damage evolution is selected and is specified as the fracture energy obtained from the polycarbonate material data sheet. The value from the material data sheet may be too low for tensile testing since the fracture energy is determined by the Izod notched impact test with a pre-notch. Since there are no pre-cracks during the tensile tests herein performed, the damage evolution value should be increased in Abaqus to match the results of the tensile tests. The authors conservatively adopted the data sheet value for the forthcoming bird strike simulations due to the lack of experimental data obtained with compatible strain rates.

3.2. Element Level

The 70 m/s speed impact history for the aluminum 2024-T42 normal and inclined plate is shown in Figure 24.

The 200 m/s speed impact results for the aluminum plate

Strain Rate (s^{-1})	0.001	0.04	0.11	1.09	2.20	3.12
True Yield Stress (MPa)	68.257	73.669	75.622	78.765	81.095	81.503
True Yield Strain	0.0641	0.0782	0.0795	0.0611	0.0651	0.0641

Table 15
True yield stress and yield strain

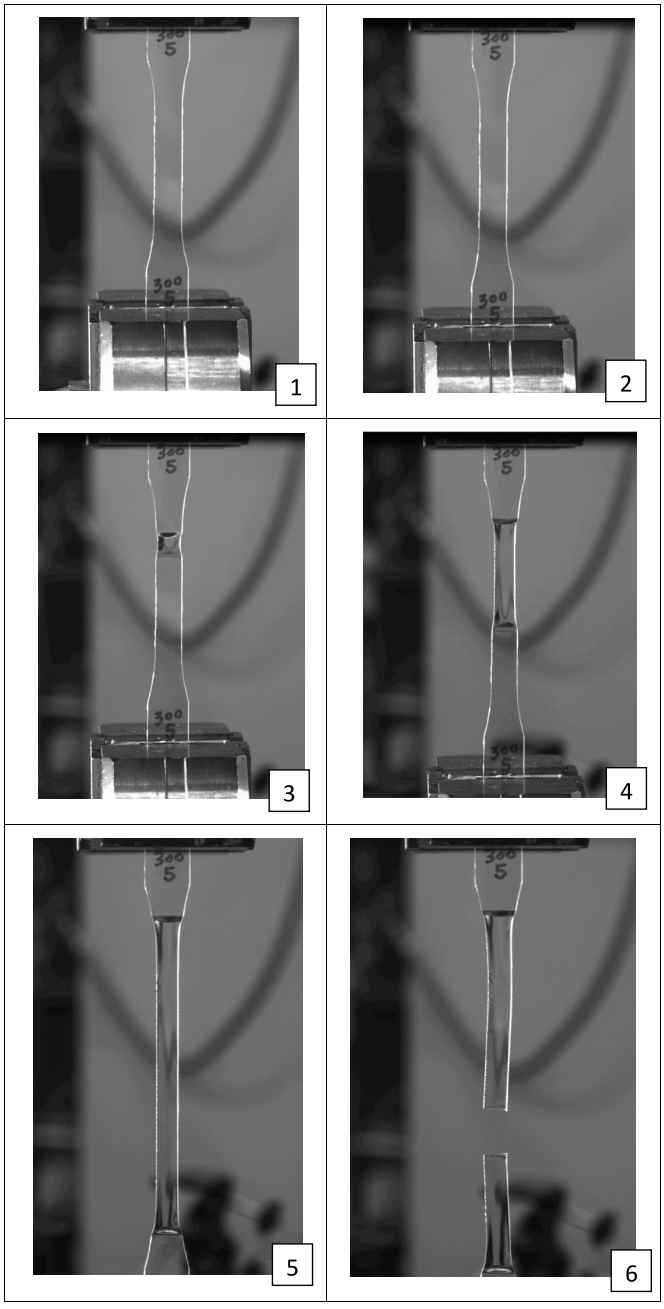

Figure 21: Tensile test loading rate 300 mm/min coupon 5 elongation history.

and the projectile is shown in Figure 25.

The 70 m/s speed impact history for the polycarbonate normal and inclined plate is shown in Figure 26.

The 200 m/s speed impact results for the polycarbonate plate is shown in Figure 27.

The theoretical duration of impact t_D is determined by using Equation 10.

$$t_D = \frac{L}{u_0} \tag{10}$$

The duration of impact is the estimated time for the travel of its full length L with an initial velocity of u_0. L for the bird is 0.2268 m and for a 70 m/s impact U_0 is 70 m/s. Thus the duration of impact for the 4lb bird at 70 m/s and 200 m/s is:

$$\begin{aligned} t_{D,70} &= 0.0032 \\ t_{D,200} &= 0.0011 \end{aligned} \tag{11}$$

From the impact sequence results, information that can be obtained are:

- The inclined impact exerts less stress on the plate due to a lower velocity component normal to the plate. The Flying-V has a sweep angle of 63.5 degrees that is larger than most commercial aircraft, which usually have a sweep angle below 40 degrees. Therefore, the Flying-V has the advantage of having less damage to the wing-fuselage leading edge, when compared to the leading edge of a conventional aircraft wing.

- After impact, the maximum stress in the plate decreases. For the inclined impact, the maximum stress location changes over time by shifting towards the plate edge.

- The initial impact of the polycarbonate plate that lasts up to 3 ms, has a more concentrated stress distribution than the aluminum 2024-T42 counterpart.

- The boundary condition of the inclined impact should not affect the impact deformation results. Since the bird mass shifts to one edge of the plate, it can be expected that a higher deformation occurs at that edge's vicinity.

The Mises stress at the centre of the plate is recorded

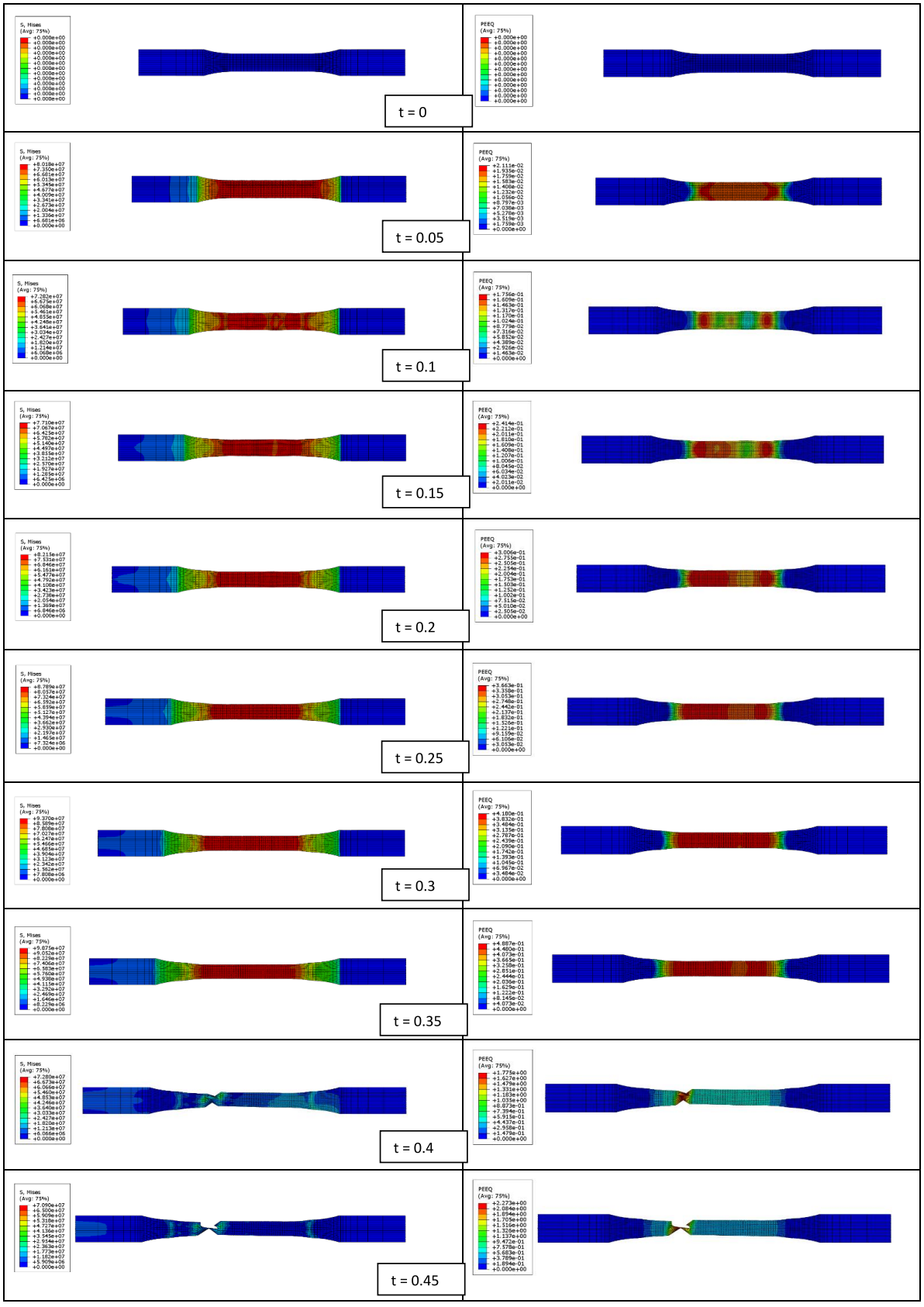

Figure 22: Abaqus dynamic explicit simulation tensile history.

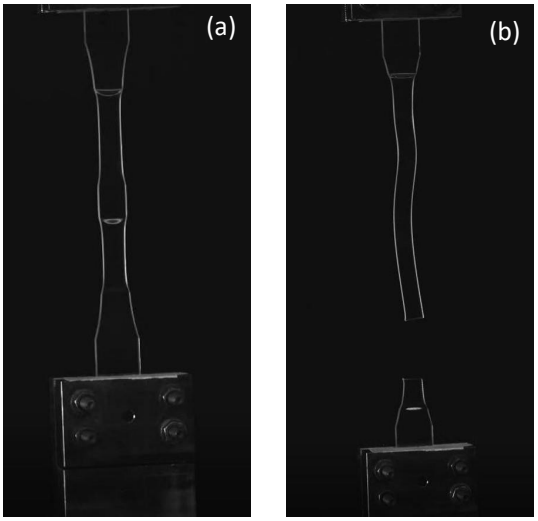

Figure 23: (a) At loading rate 7500 mm/min two location necking occurs. (b) At loading rate 30000 mm/min coupon's wave-shaped deformation after fracture.

for each impact scenario, as shown in Figure 28 (a) and Figure 28 (b). The horizontal axis is normalized impact time, which is the impact time divided by the duration of impact $t_{D,70}$ and $t_{D,200}$ in Equation 11. The value 1 on the horizontal time means that the bird has fully impacted the plate. The stress and energy values after 1 are the response of the plate after impact. It is shown that the aluminum plate generated higher peak stresses than the polycarbonate plate. After the impact duration, the peak stresses in the aluminum plate decays whereas the stress in the polycarbonate retains its peak value during impact. For the inclined plates, it is shown that the stress in the centre gradually decays then stabilizes since the bird's mass is shifting to the plate's edge. Thus, changing the location of the peak stress. This effect is more significant in aluminum than polycarbonate. The plate's internal energy (ALLIE) history during impact is plotted in Figure 28 (c) and Figure 28 (d). The stored elastic strain energy (ALLSE) is the main contributor of ALLIE. Therefore, the energy history plotted can be viewed as elastic strain energy. During the normal and inclined impact, polycarbonate showed its ability to absorb the most amount of energy, three times higher at the peak of the impact duration. When the deformation reaches the maximum, the internal energy and centre stress also reaches maximum while the dynamic energy is minimum.

3.3. Detail Level

The purpose of the detail level is to construct an initial working model for the bird strike simulation. The elastic strain (ALLSE) and the plastic strain (ALLPD) history is presented to compare the amount of energy absorbed in the structural component, shown in Figure 29 and Figure 30. The bird strike stress distribution history is shown in Figure 31.

Plastic strain is generated in the window frame and fuselage skin. The plastic strain in the pane is at the scale of 10^{-3}, which can be ignored while the highest plastic strain is generated in the window frame. There are two phases of peaks in the ALLSE history, the first peak is at the time of the bird impacting the windowpane at its duration of impact. The second peak is when the bird slides along the windowpane and impacts the window frame and skin. Since the frame has a higher thickness and stiffener geometry, it deforms less resulting in a lower ALLSE peak. After 14ms, the bird material has no contact with the structure, the stored elastic energy releases with some residual elastic energy. The limitation in the detailed level that prevents it from generating trustworthy data is the lack of stiffening members around the fuselage skin. Another limitation of the detailed model is the undetected behaviour of its vicinity window sections. In Figure 31, after 14ms, the bird material is supposed to move to the other window section creating new stresses and plastic strain distribution but the adjacent window and fuselage structure are absent. Therefore, from the detailed level results, it is learned that a second window section should be added in the sub-component level model.

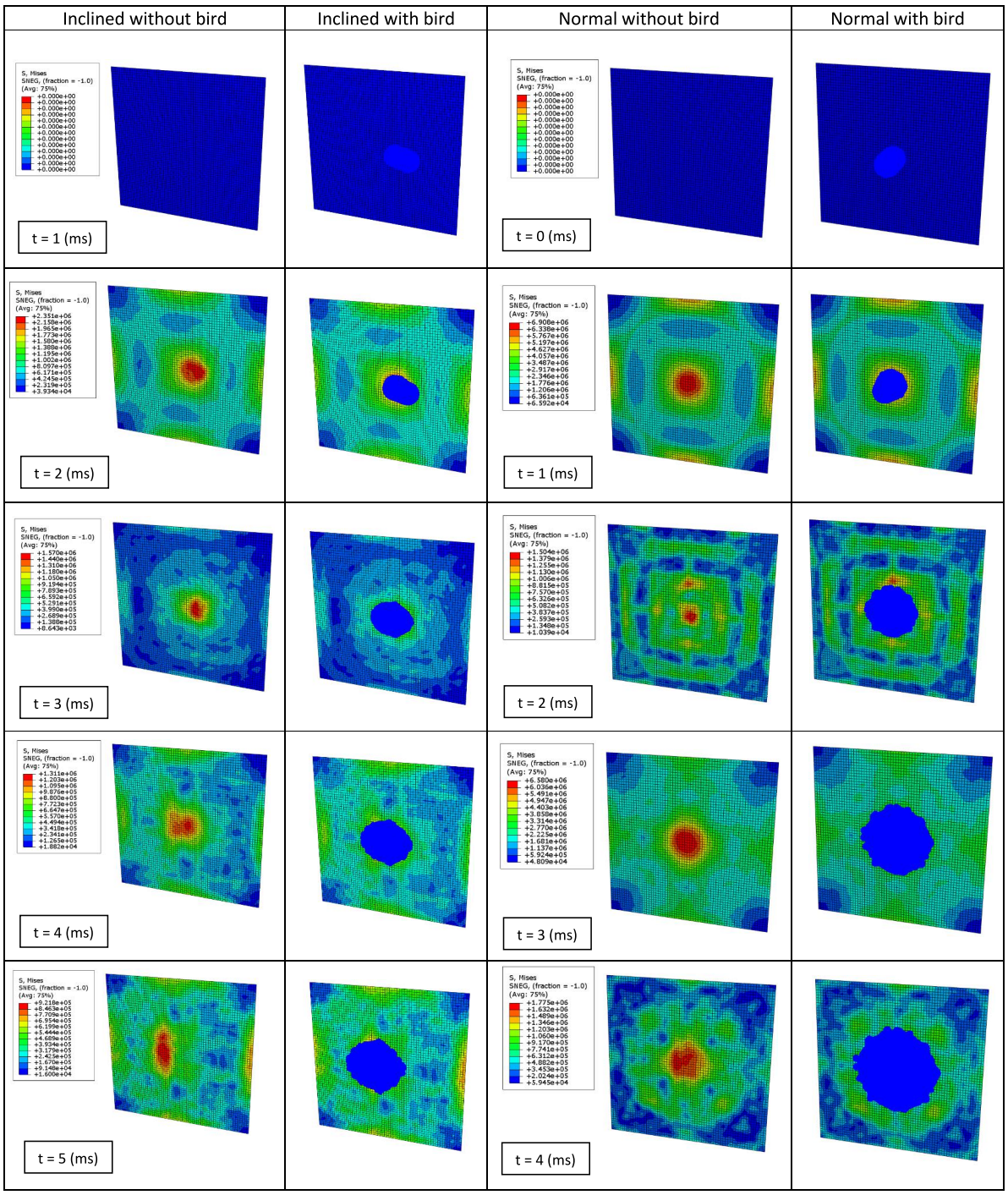

Figure 24: Normal and inclined aluminum 2024-T42 70 m/s impact sequence

3.4. Sub-Component Level

3.4.1. Fuselage Frame Impact

Figure 32 and Figure 33 show the elastic and plastic energy impact history of the fuselage frame. Although the middle fuselage impact has the highest peak strain energy, it doesn't have the highest plastic energy. The highest plastic strain energy of 14J occurs in the impact located at the centre fuselage frame, while the top impact has the lowest plastic energy.

The plastic energy of the centre impact can be further inspected by its contributors in the window structure shown in Figure 34. The main contributor is the fuselage skin at

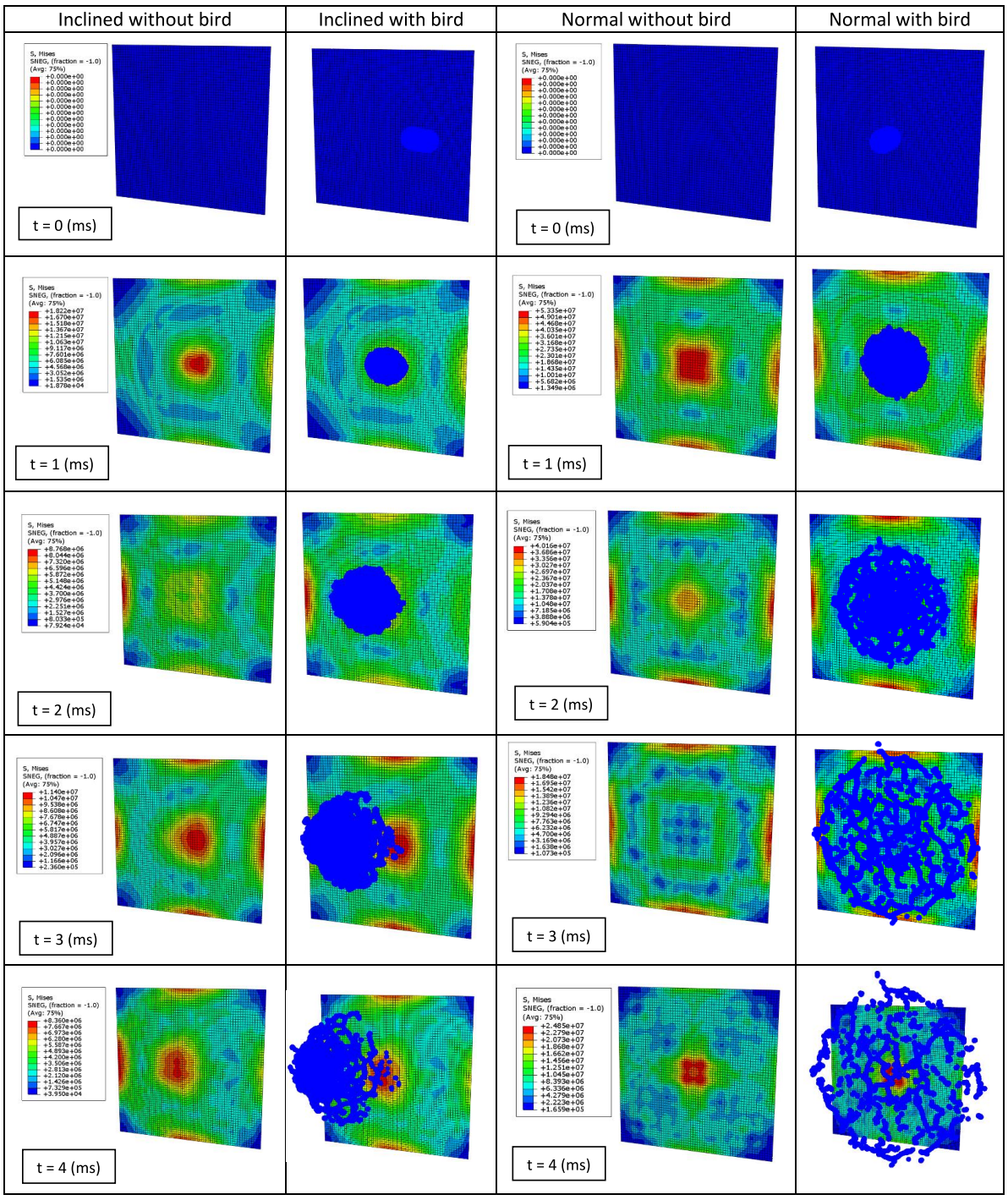

Figure 25: Normal and inclined aluminum 2024-T42 200 m/s impact sequence

section 1 and the window frame at section 2. The contribution of the elastic strain is also shown in Figure 35, where the fuselage skin (skin1/pink) has the highest contribution at the first peak and after the second peak.

The first peak is at the time of the bird's impact duration, and the second peak is at the bird having contact with the second window pane (pane2/green) and window frame (frame2/white). The energy peaks is illustrated with the motion of the bird materials and the Mises stress distribution from t=0 ms to t=18 ms shown in Figure 36.

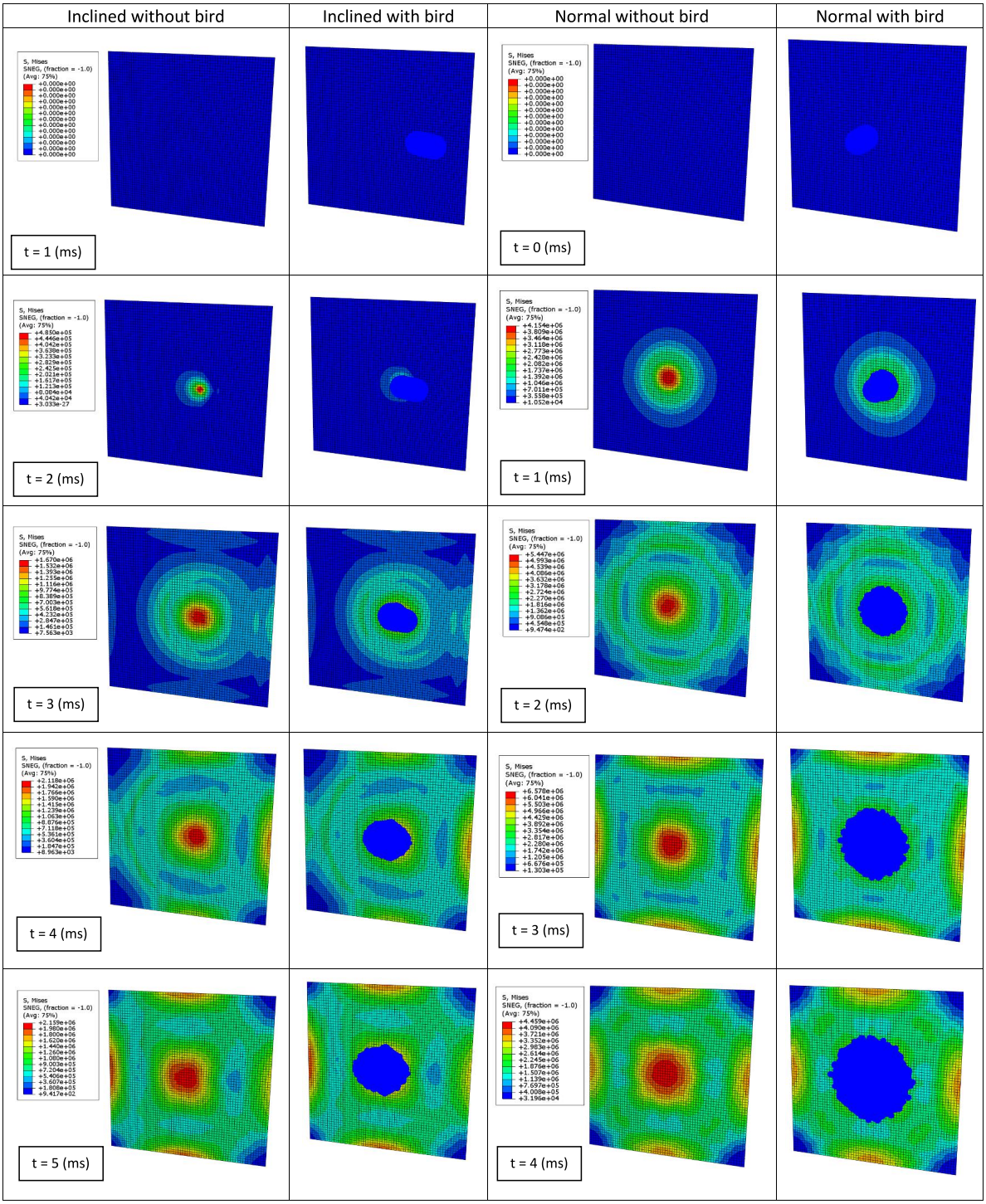

Figure 26: Normal and inclined polycarbonate 70 m/s impact sequence.

3.4.2. Passenger Window impact

The location numbering of the window impact is shown in Figure 17. The window impact location will be compared horizontally (1-4, 10-12), vertically (1, 5-9) and diagonally (13-16) by using the energy method.

For the horizontal impact, it is shown in Figure 37 that the centre impact generates the highest amount of plastic energy. It also generates the highest peak of the internal energy shown in Figure 38 since it is the location furthest away from the window frames. Impact location 2, 3, 4 generates a lower

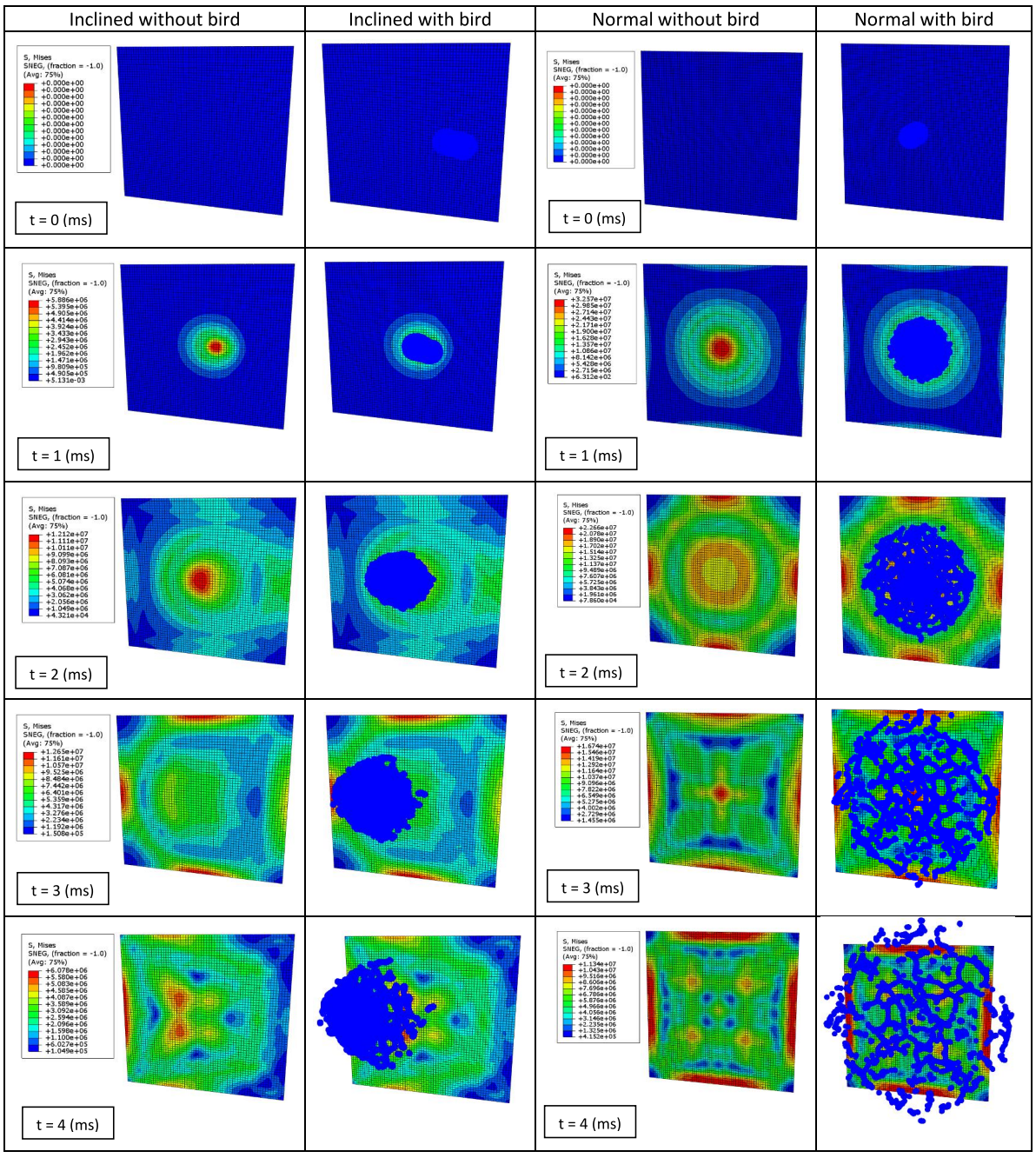

Figure 27: Normal and inclined polycarbonate 200 m/s impact sequence

amount of plastic energy than location 10, 11, 12 since for 2, 3, 4 the bird material slides to the stiffer skin-fuselage structure rather than 10, 11, 12 which the bird slides to the other side of the window frame and fuselage skin. To conclude, the critical location of the horizontal window impact is location 1.

For the vertical impact, location 6 is the most critical point that generates the highest amount of plastic energy shown in Figure 39. Starting from location 1 (centre of the window) moving upwards, the generated plastic energy increases until it reaches location 7 which is closer to the window frame. Moving above location 7, the plastic strain generated will decrease since the bird material is interacting less with the window structure. The internal energy ALLIE dur-

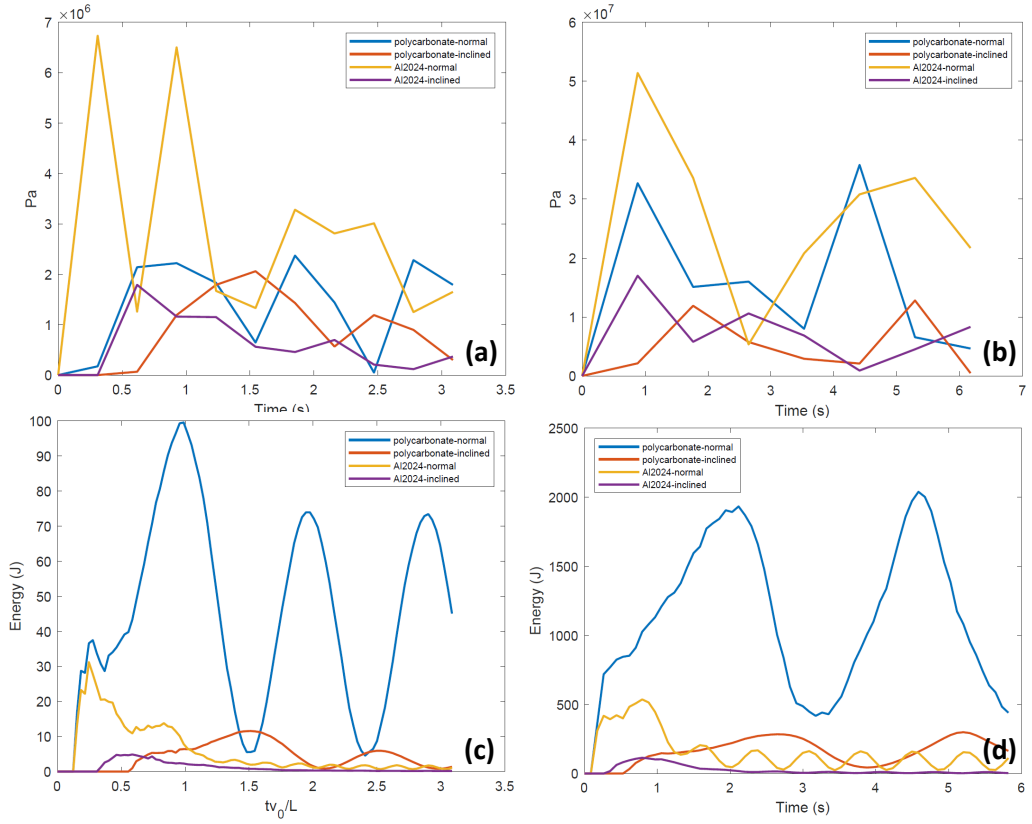

Figure 28: (a) Pressure comparison of 70m/s thick plate impact. (b) Pressure comparison of 200m/s thick plate impact. (c) ALLIE comparison of 70m/s thick plate impact. (d) ALLIE comparison of 200m/s thick plate impact

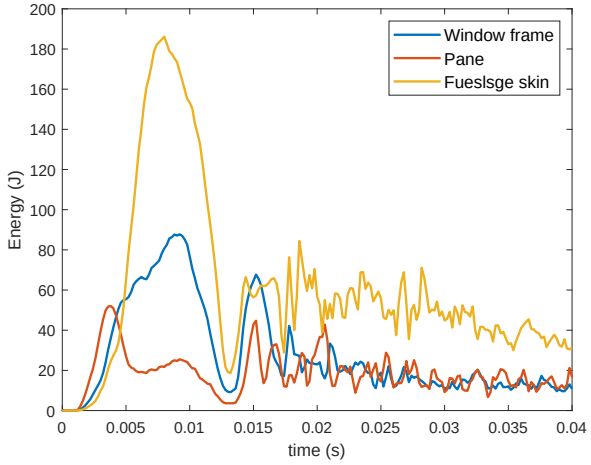

Figure 29: ALLSE in the structure components

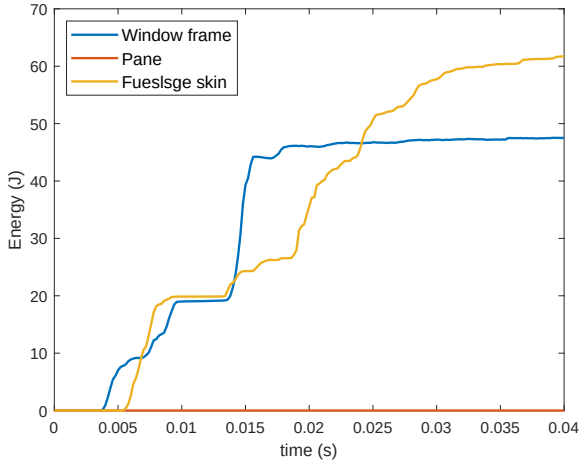

Figure 30: ALLPD in the structure components

ing the impact history is shown in Figure 40. The window centre has the highest peak although is doesn't has the highest ALLPD.

For the diagonal impact, location 15 has the highest amount of plastic energy shown in Figure 41. Location 15 generated a higher amount of plastic energy than location 13. This is similar to the results in the horizontal impact which the impact of the right half side window has more damage than the

right. The internal energy ALLIE is shown in Figure 42.

Note that location 12 and location 16 is not impacted at the location shown in Figure 17 but at the updated location in Figure 43. The reason to switch locations 12 and 16 to section 2 is due to the impacting location being too close to the skin panel boundary which does not have any fuselage frame. The deformation of the skin panel and the window frame is too high that the bird will penetrate through the window. A more realistic approach would be impacting 12 and 16 at window section 2 so that there is support from the fuselage frame.

To conclude, the critical impact location within the three study groups are location 1 for the horizontal impact, location 6 for the vertical impact, and location 15 for the diagonal impact. Among those three points and the fuselage frame impact points, location 6 has the highest amount of plastic energy with a value approximately of 370J. Location 6 is therefore determined as the critical impact point of the Flying-V leading-edge fuselage. The energy contribution for each structural elements of ALLPD and ALLIE at location 6 is shown in Figure 44 and Figure 45. The window frame (yellow), polycarbonate pane, pane clamp and fuselage skin are the main contributors to the plastic strain energy while the pane clamp has the highest value. The impact history of location 6 is shown in Figure 46.

3.4.3. Reduced Integration - Hourglass Mode

In all the sub-component simulations, the reduced integration is turned off. It is important to mention that the default setting in Abaqus has the reduced integration turned on. When the reduced integration is turned on, hourglass modes may occur to the linear finite elements during element in-plane bending or twist warping. Although there is excessive element deformation that requires energy, the internal energy of the element has not changed. The artificial strain energy (ALLAE) is added in ALLIE as the energy for element deformation that is not recorded due to the hourglass effect. By turning off reduced integration, the hourglass effect is eliminated, making the stress and strain results more accurate. To obtain a reliable output result, the ratio of artificial strain energy to internal energy (ALLAE/ALLIE) should be below 5% [18]. A more rigorous criteria that the authors recommend is to keep this ratio below 2%. The ratio of ALLAE to ALLIE is shown in Figure 47, which remains below 2% throughout the impact history when reduced integration is turned off. The small residual value of about 0.5% comes from the drilling penalty factor used in the shell formulation. The authors recommend to turn off the reduced integration option when performing bird strike simulations, although resulting in computationally more expensive simulations. Whenever reduced integration is to be used, one should first evaluate whether the accuracy of the results generated by reduced integration is accepted, by observing the criterion (ALLAE/ALLIE) lower than 2%.

3.4.4. Sensitivity Analysis

The critical impact location identified for the Flying-V, location 6, is chosen for the sensitivity analysis. An additional fuselage frame and the shear clip are added at the section 1 edge shown in Figure 48, since in reality there should be a fuselage frame structure at that location. By adding those stiff structure components, the plastic strain energy ALLPD could be decreased by 15%, as shown in Figure 49.

The sensitivity analysis is done by adjusting the thickness for one structural component at a time to examine the values of the total model weight and ALLPD history in the model. The weight of the total model is calculated using Table 16 as an example for the baseline geometry, noting that the 2 multiplier appears because there are two components in the model. The baseline thicknesses are the thickness values

Component	Area(m2)	Density (kg/m3)	Baseline Thickness	Baseline Thickness Weight (kg)
2×Skin	0.52	2770	0.0025	7.202
2×Window Frame	0.241	2800	0.003	4.0488
2×Pane Clamp	0.141	2800	0.003	2.3688
2×Pane	0.133	1200	0.0096	3.06432
2×Clamp Fastener	0.095	2800	0.002	1.064
2×Fuselage Frame	0.117	2770	0.0025	1.62045
2×Fuselage Frame Shear Clip	0.064	2770	0.0025	0.8864
2×Stringer	0.082	2770	0.0025	1.1357

Table 16
Weight calculation of the total model using the baseline component thickness.

(mm)	Baseline Thickness	Thickness 2	Thickness 3	Thickness 4	Thickness 5
Skin	0.0025	0.003125	0.00375	0.004375	0.005
Window Frame	0.003	0.00375	0.0045	0.00525	0.006
Pane Clamp	0.003	0.00375	0.0045	0.00525	0.006

Table 17
Thickness variables for the sensitivity study.

defined in Table 9. The baseline weight is the multiplication of the area density and thickness. In the weight sensitivity analysis, 5 (five) thickness variables are applied including the first baseline thickness. Three structural components are used to study the sensitivity, the skin, window frame and the pane clamp. Their 5 (five) thicknesses are shown in Table 17. The total model weight calculated is shown in Table 18. Using Table 18, the weight sensitivity for each component is plotted in Figure 50.

The weight sensitivity is correlated with the surface area of the components. Since the fuselage has the highest surface area, it has the highest weight sensitivity. For each varied component thickness, a simulation is performed in which the maximum ALLPD value is retrieved from the ALLPD history plots and the plastic energy sensitivity to the component thickness is shown in Figure 51.

From Figure 51, it is shown that the ALLPD of the skin component is least sensitive to the thickness increase, which has the highest effect on the weight. Therefore, increasing the skin weight to reduce plasticity will increase weight and not be effective in reduce the plastic behaviour under bird strike. The highest plastic energy sensitivity is about the thickness of the pane clamp, indicating that reinforcing the structure that clamps the pane can decrease plasticity effectively. Interestingly, the pane clamp thickness has the lowest effect on the weight, being yet another reason to be the recommended component for thickness increment. The authors investigated a case where the panel clamp thickness is increased by a factor of two, not yet leading to a plasticity-free design, but instead decreasing the plasticity by 50%.

A method to further decrease plasticity is to apply different thickness combinations by increasing the thickness of the window frame and the pane clamp simultaneously. To apply this method, the window frame thickness is chosen to be 3.75mm and the pane clamp as 5.25mm is since higher thickness did not make a large difference in plasticity. By combining the two components with the designated thickness, it is shown in Figure 52 that the ALLPD can be further decreased to 80J. Although the model is still not plastic-free, a significant plasticity decrease is achieved. Further improvement in the plasticity behaviour is not pursued in the present study, which could be achieved extending the methodology herein developed and applying it within an optimization framework. Nevertheless, sensitivity analyses such as the one herein performed are of utmost importance to gain insight about the design and possible directions of improve-

Total model weight (kg)	Baseline Thickness	Thickness 2	Thickness 3	Thickness 4	Thickness 5
Skin variable	21.39047	23.19097	24.99147	26.79197	28.59247
Window frame variable	21.39047	22.40267	23.41487	24.42707	25.43927
Pane Clamp variable	21.39047	21.98267	22.57487	23.16707	23.75927

Table 18
Total model weight calculated by the component's adjusted thickness.

ment.

3.5. High-speed impact speed

A 4lb bird with an impact speed of 133.38 m/s, which is the cruising speed of the Flying-V at 37000 ft, is simulated using the improved model obtained from the sensitivity analysis. Figure 53 shows that the window has a large displacement and even that penetration occurred. Since this is an extreme impact scenario, only the damage mode is presented, and no further attempts to improve the design are performed. Possible solutions that could have been further investigated for this observed penetration are: fasten the polycarbonate pane with fasteners; apply adhesive before clamping the window pane.

4. Conclusions

A design based on a Mitsubishi Aircraft Corporation passenger window patent was proposed for the Flying-V wing-fuselage windows, which are exposed to the flight direction and subject to bird strike. The bird model herein adopted consisted of a smoothed particle hydrodynamics (SPH) model using gelatin material properties to simulate the bird constitutive behavior. During a bird strike on the passenger window, the impact location above and below the window pane's centre was the most critical point, showing maximum plastic deformation. During a bird strike on the fuselage where the fuselage frame is located, the centre of the leading edge is the most crucial impact location.

The fuselage skin, window frame and pane clamp are used for the weight and plastic energy sensitivity analysis. The pane clamp thickness showed the highest plasticity sensitivity, and doubling its thickness resulted in a 50% decrease in the maximum plastic energy, to 150J. Further reduction in the plastic deformation was achieved by increasing the thicknesses of the pane clamp and the window frame. By increasing the window frame thickness from 3mm to 3.75mm, and the pane clamp from from 3mm to 5.25mm, the plasticity energy decreases to 80J. Although the obtained design was not plasticity-free, using the results from the sensitivity analysis decreased the plastic energy in the design by a total of 80%. The improved design was impacted with a 4lb bird with a velocity 0f 133 m/s, which is the cruising speed of the Flying-V at 37000 ft. This altitude is the highest bird strike altitude ever recorded, showing a critical impact scenario for which the passenger window was penetrated. Therefore, further analysis and design iterations are required before reaching a feasible design for the Flying-V.

Recommendations for Future Work

The building block approach herein presented will be further developed and coupled within an optimization framework with the aim to automate the design changes herein performed by means of sensitivity analyses. Every change in the geometry requires a re-designation of the material, section assignments, surface, geometry and node sets. Every change in the thickness of the component requires the translation of the components to avoid overlapping of the rendered shell thickness. An automatic method should be developed to decrease the modelling time during automated design iterations.

Physical testing at the element level and the detailed level should be performed to validate the proposed simulation models. Since testing requires more time and budget investment compared to simulation, a funded research will be required for such activities.

It is recommended to break down the window frame, pane clamp, clamp fastener components into numerous number of flanges and perform a more extensive sensitivity analysis, and optimization capability. Such design parameterization should allow changing the length and thickness of the flanges, for instance. Fastening the window pane to the window frame rather than having it clamped is a design modification that is expected to improve the 133 m/s high-speed impact.

Acknowledgements

This research study is supported by Fokker Aerostructures B.V. and the Aerospace Engineering faculty at Delft University of technology. The author would to thank all those who contributed their aid to this project. Wydo van de Waerdt for contributing the insight of constructing a BBA for bird strike analysis and feedback of the simulation results. Professor Boyang Chen, Luc Kootte, and Jan Hol for solving issues of Abaqus running on the TU Delft cluster service. This research received no external funding.

Conflict of interest

The authors declare that they have no conflict of interest.

CRediT authorship contribution statement

Sian Ying Chen: Methodology, software, formal analysis, investigation, validation, writing - original draft preparation, writing - review and editing. **Wydo van de Waerdt:** Methodology, supervision, writing - review and editing. **Saullo G. P. Castro:** Conceptualization, methodology, supervision, writing - review and editing.

References

[1] , July 2016. Metallic materials properties development and standardization (MMPDS): MMPDS-11. Battelle Memorial Institute., William J. Hughes Technical Center (U.S.), United States. URL: http://app.knovel.com/web/toc.v/cid:kpMMPDSM74/viewerType:toc/root_slug:metallic-materials-properties.

[2] Agency, E.U.A.S., 2020. Certification specifications and acceptable means of compliance for large aeroplanes cs-25. URL: https://www.easa.europa.eu/downloads/121128/en8.

[3] Belytschko, T., Liu, W.K., Moran, B., Elkhodary, K., 2014. Nonlinear Finite Elements for Continua and Structures. 2nd ed., John Wiley & Sons Ltd. URL: https://www.wiley.com/en-us/Nonlinear+Finite+Elements+for+Continua+and+Structures%2C+2nd+Edition-p-9781118632703#description-section.

[4] Benad, J., 2015. Design of a commercial aircraft for high-subsonic speed as a flying wing configuration. Msc thesis. Technical University of Berlin. Berlin.

[5] Dotman, T., 2021. A Structural Sizing Methodology for the Wing-Fuselage of the Flying-V. Ph.D. thesis. Delft University of Technology. URL: http://resolver.tudelft.nl/uuid:69e21e65-7168-4f83-abf5-b646bb4c7fe5.

[6] El-Sayed, A.F., 2019. Bird strike in aviation: statistics, analysis and management. John Wiley & Sons Ltd. URL: https://search.ebscohost.com/login.aspx?direct=true&scope=site&db=nlebk&db=nlabk&AN=2141844.

[7] Fu, S., Wang, Y., Wang, Y., 2009. Tension testing of polycarbonate at high strain rates. Polymer Testing 28, 724–729. URL: https://www.sciencedirect.com/science/article/pii/S0142941809001020, doi:https://doi.org/10.1016/j.polymertesting.2009.06.002.

[8] Goyal, V., Huertas, C., Borrero, J., Leutwiler, T., 2006a. Robust Bird-Strike Modeling Based on ALE Formulation Using LS-DYNA, in: 47th AIAA/ASME/ASCE/AHS/ASC Structures, Structural Dynamics, and Materials Conference 14th AIAA/ASME/AHS Adaptive Structures Conference 7th, American Institute of Aeronautics and Astronautics, Reston, Virigina. URL: http://arc.aiaa.org/doi/abs/10.2514/6.2006-1759, doi:10.2514/6.2006-1759.

[9] Goyal, V., Huertas, C., Leutwiler, T., Borrero, J., Vasko, T., 2006b. Robust Bird-Strike Modeling Based on SPH Formulation Using LS-

DYNA, in: 47th AIAA/ASME/ASCE/AHS/ASC Structures, Structural Dynamics, and Materials Conference 14th AIAA/ASME/AHS Adaptive Structures Conference 7th, American Institute of Aeronautics and Astronautics, Reston, Virigina. URL: http://arc.aiaa.org/doi/abs/10.2514/6.2006-1878, doi:10.2514/6.2006-1878.

[10] Mitsubishi Aircraft Corporation-Aichi (JP), T.Y., 2012. Aircraft window. URL: https://patents.google.com/patent/US9415854?oq=12178442.5.

[11] Niu, C., Niu, M., 1999. Airframe Structural Design: Practical Design Information and Data on Aircraft Structures. Airframe book series, Adaso Adastra Engineering Center. URL: https://books.google.nl/books?id=yT15SwAACAAJ.

[12] Nizampatnam, L.S., 2007. Models and methods for bird strike load predictions. phd thesis. URL: https://soar.wichita.edu/handle/10057/1494.

[13] Oosterom, W., 2021. Flying-v family design. URL: https://repository.tudelft.nl/islandora/object/uuid%3A9e8f9a41-8830-405d-8676-c46bf6b07891.

[14] Plast, A., 2014. Transparent products polycarbonate sheets makroclear. URL: https://arlaplast.com/wp-content/uploads/2021/05/Datasheet-Makroclear-2014-EN-v1.pdf.

[15] Reza Hedayati, M.S. (Ed.), 2016a. Bird Strike An Experimental, Theoretical, and Numerical Investigation. 2 - Statistics. Woodhead Publishing. URL: https://doi.org/10.1016/B978-0-08-100093-9.00002-9, doi:10.1016/B978-0-08-100093-9.00002-9.

[16] Reza Hedayati, M.S. (Ed.), 2016b. Bird Strike An Experimental, Theoretical, and Numerical Investigation. 6 - Finite element bird strike modeling. Woodhead Publishing. URL: https://doi.org/10.1016/B978-0-08-100093-9.00002-9, doi:10.1016/B978-0-08-100093-9.00002-9.

[17] Ritt, S., 2021. Sae g-28 simulants for impact and ingestion technical strategy.

[18] Smith, M., 2009. ABAQUS/Standard User's Manual, Version 6.9. Dassault Systèmes Simulia Corp, United States.

[19] TUDOR, A., 1968. Bird ingestion research at rolls-royce(aircraft gas turbine engine damage from bird ingestion, discussing bird simulation tests, flight hazards and engine design implications).

[20] Verma, A.S., Castro, S.G., Jiang, Z., Teuwen, J.J., 2020. Numerical investigation of rain droplet impact on offshore wind turbine blades under different rainfall conditions: A parametric study. Composite Structures 241, 112096. doi:10.1016/j.compstruct.2020.112096.

[21] Wilbeck, J.S., 1977. Impact behavior of low strength projectiles. Ph.D. thesis. Texas A&M University.

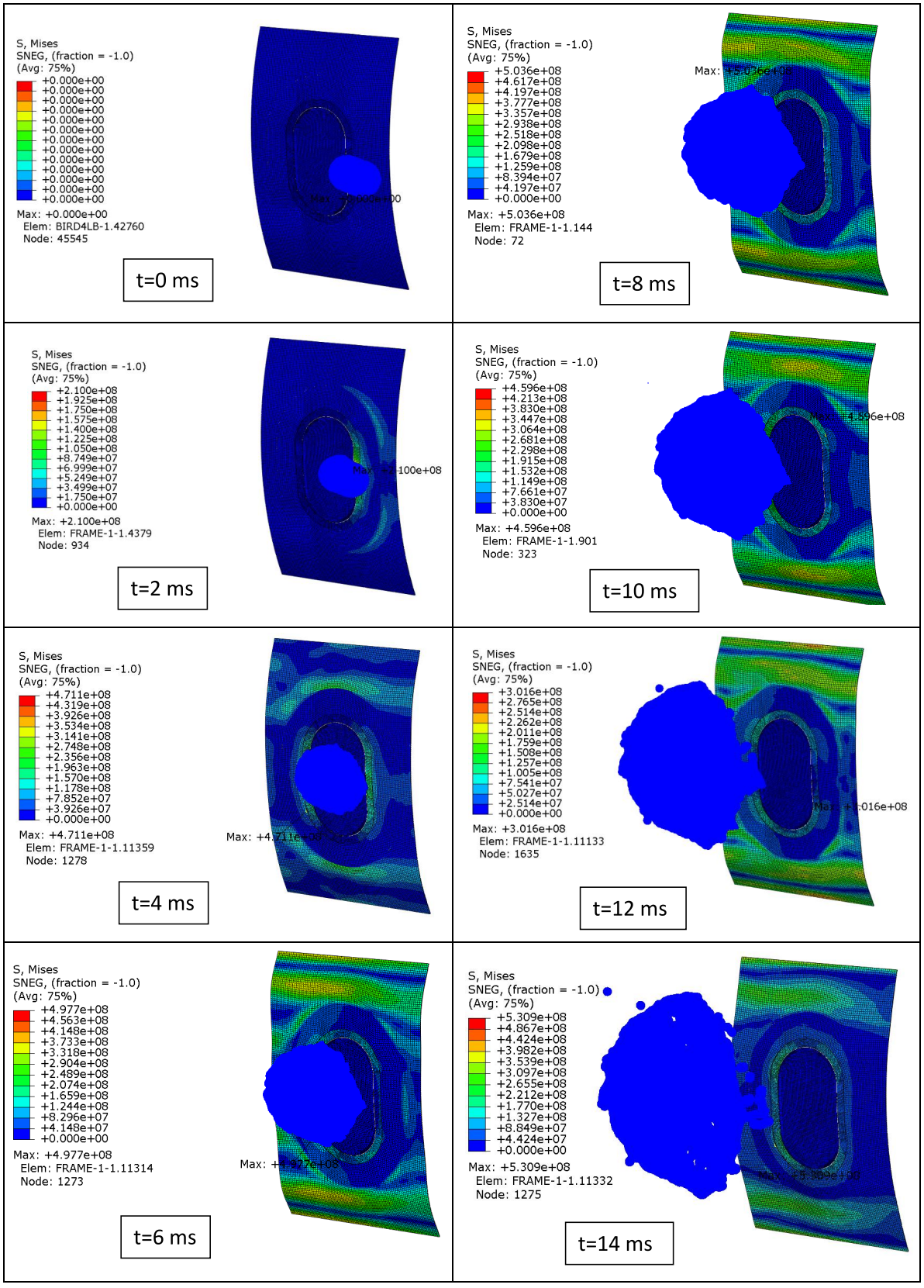

Figure 31: Detailed level 70 m/s bird strike stress distribution.

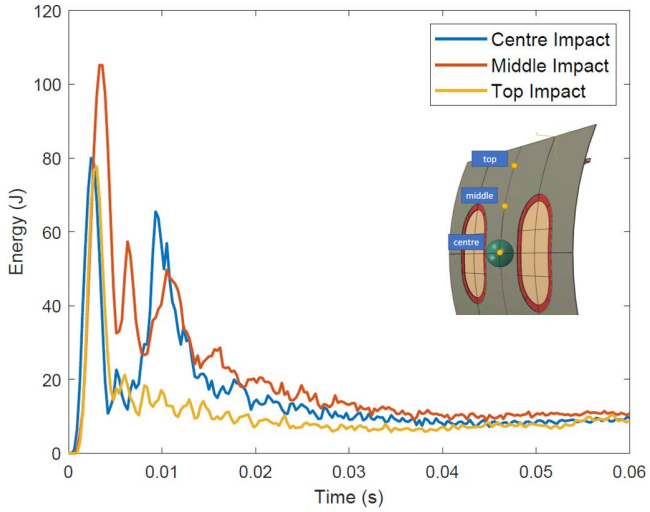

Figure 32: Fuselage frame impact ALLSE comparison.

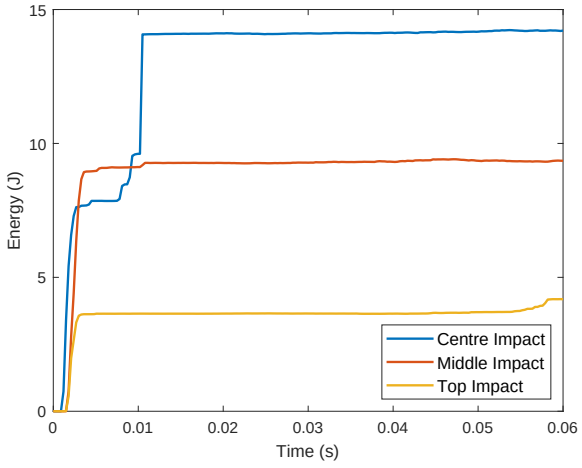

Figure 33: Fuselage frame impact ALLPD comparison.

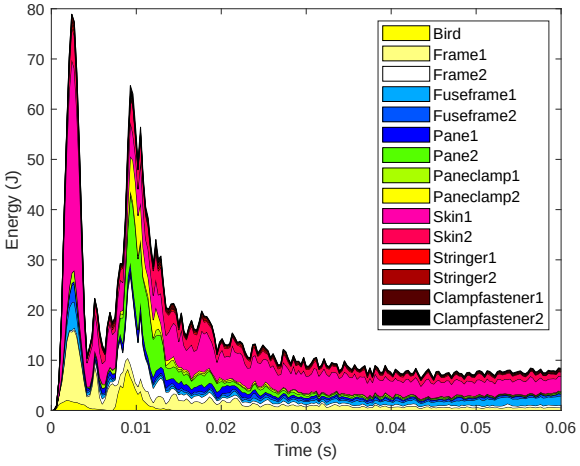

Figure 35: Centre impact ALLSE contributors.

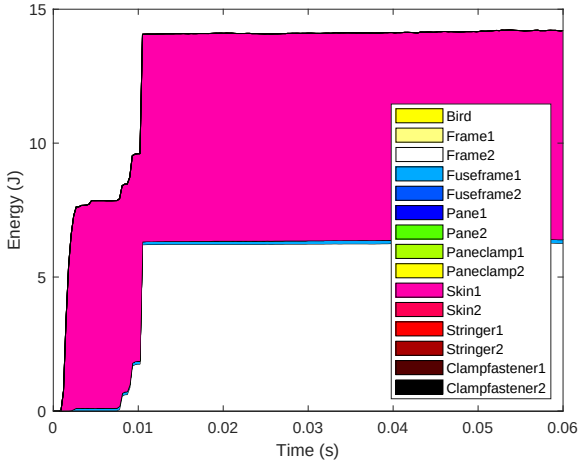

Figure 34: Fuselage frame centre impact ALLPD contributors.

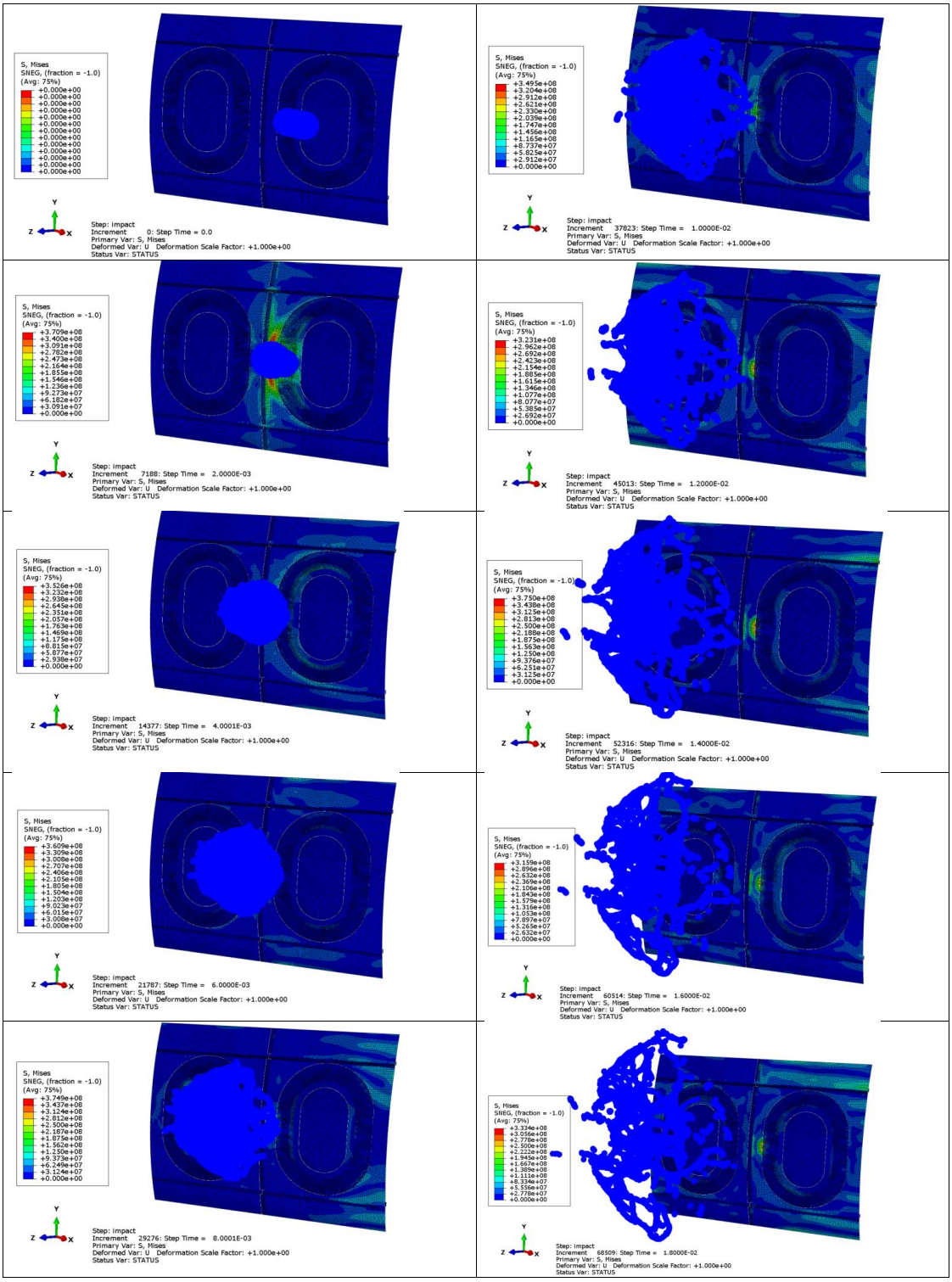

Figure 36: Impact sequence of the fuselage frame centre impact.

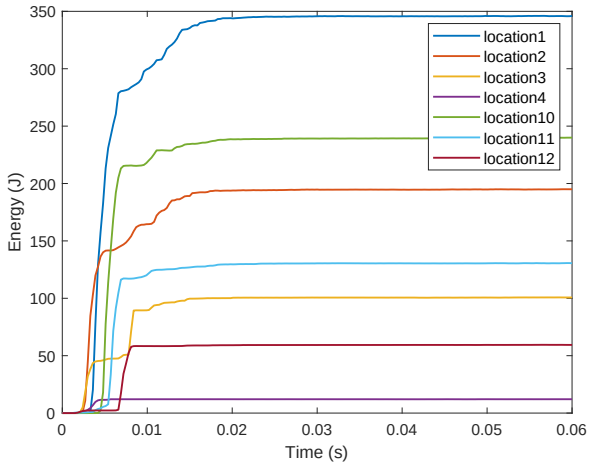

Figure 37: ALLPD horizontal impact location comparison

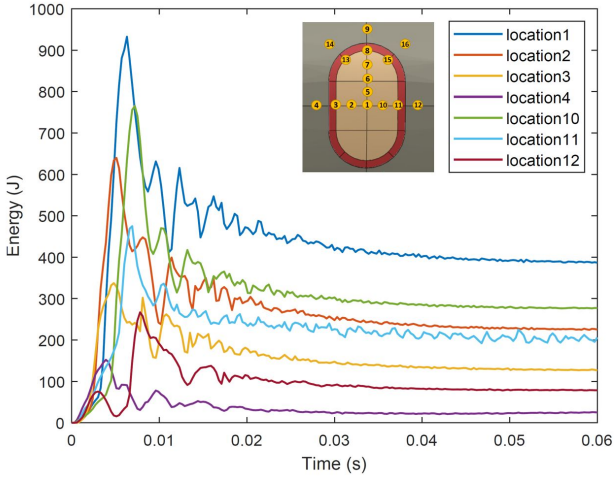

Figure 38: ALLIE horizontal impact location comparison

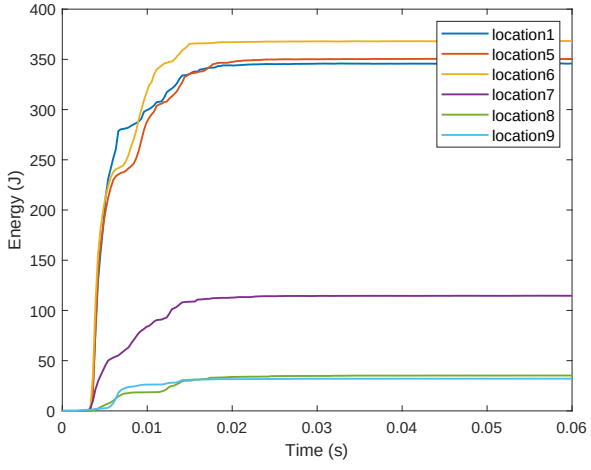

Figure 39: ALLPD vertical impact location comparison

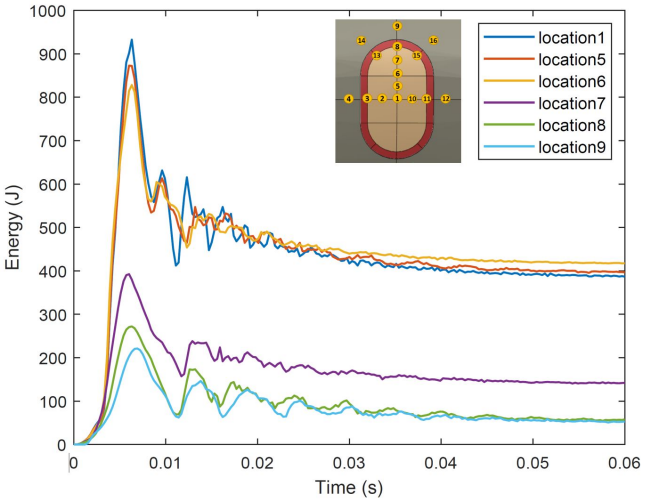

Figure 40: ALLIE vertical impact location comparison

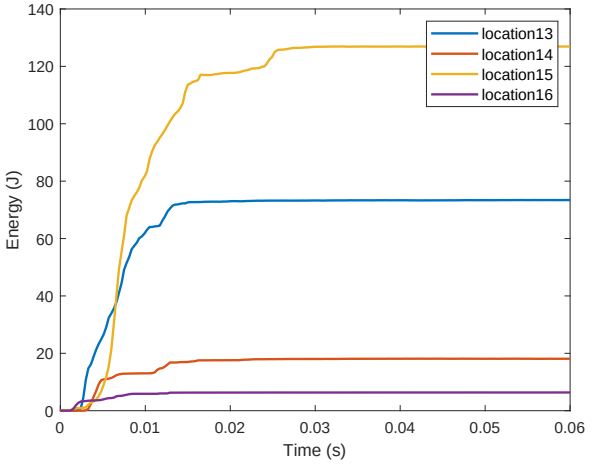

Figure 41: ALLPD diagonal impact location comparison

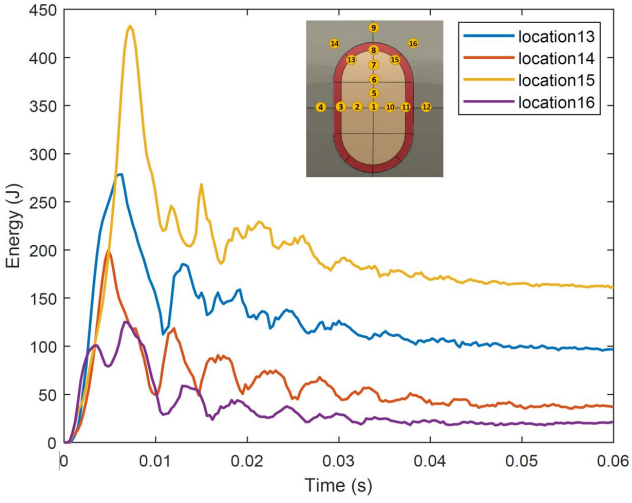

Figure 42: ALLIE diagonal impact location comparison

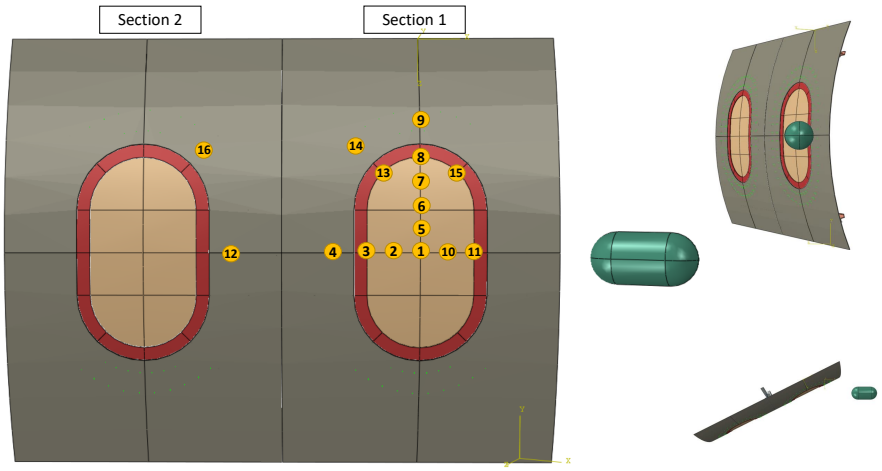

Figure 43: Passenger window 16 impact updated location study.

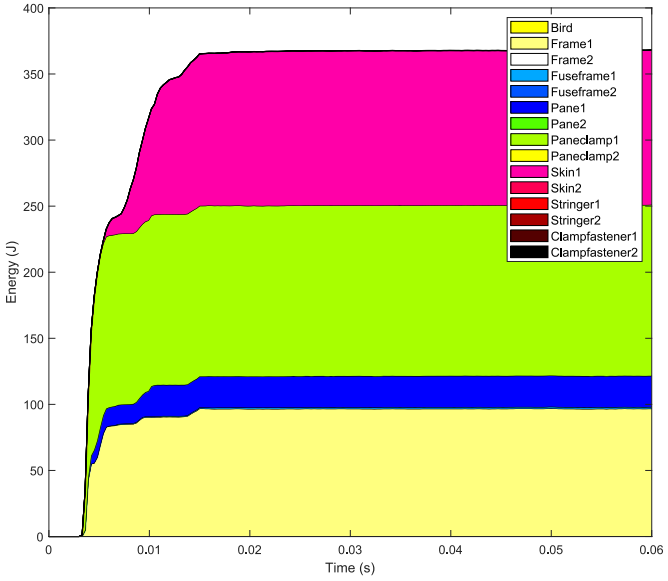

Figure 44: Location 6, critical impact point ALLPD contributors

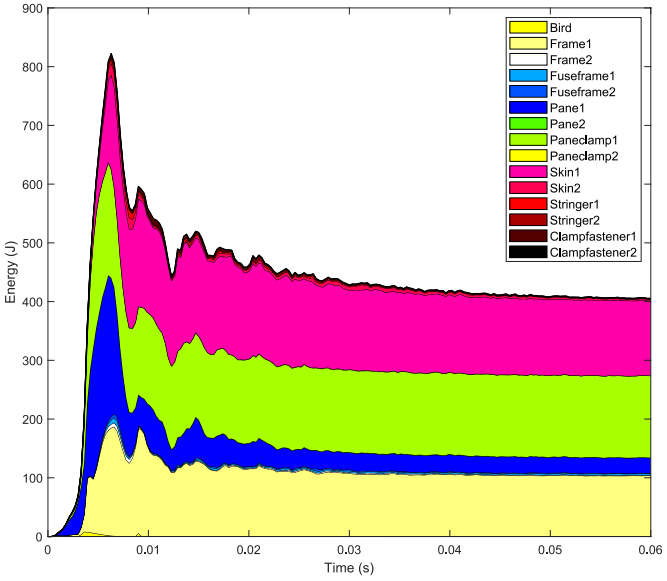

Figure 45: Location 6, critical impact point ALLIE contributors

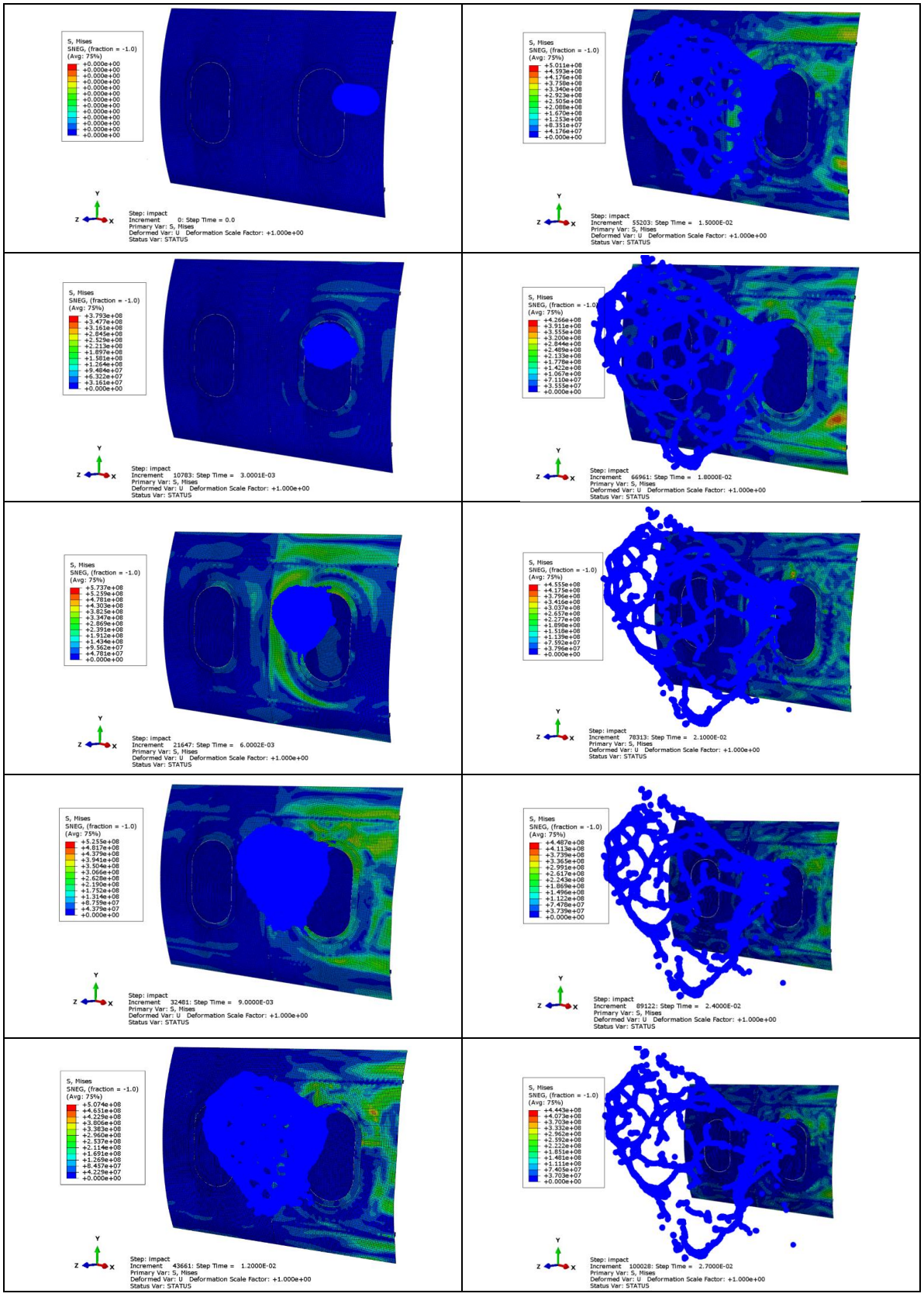

Figure 46: Critical impact location 6 impact sequence

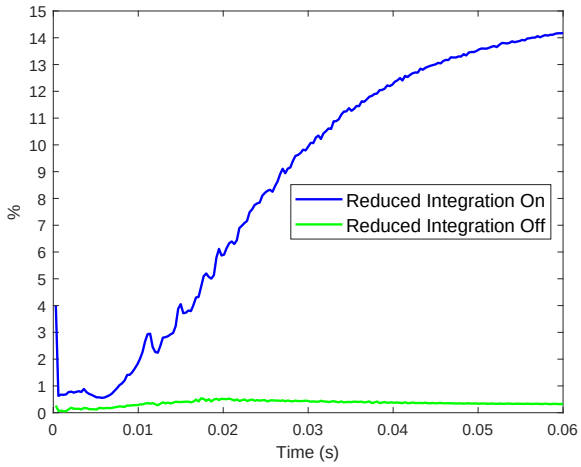

Figure 47: Artificial strain energy to elastic strain energy ratio.

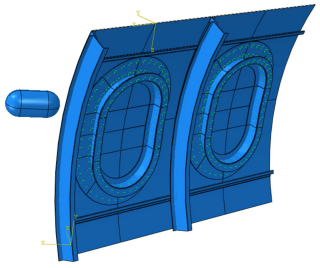

Figure 48: Model for sensitivity analysis with two fuselage frames.

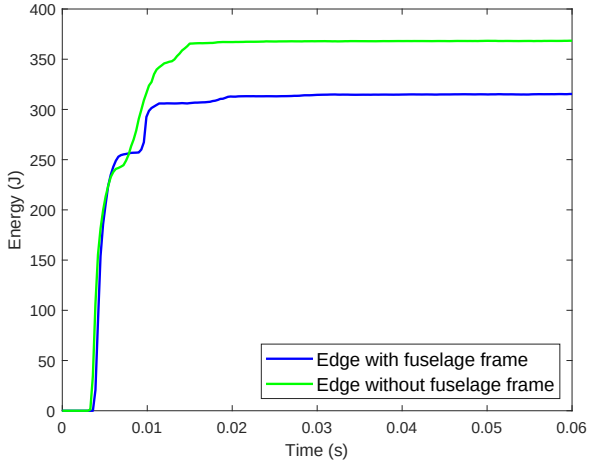

Figure 49: ALLPD comparison for adding fuselage at section 1 edge. Adding an additional frame at the edge can decrease maximum plastic energy for 15%

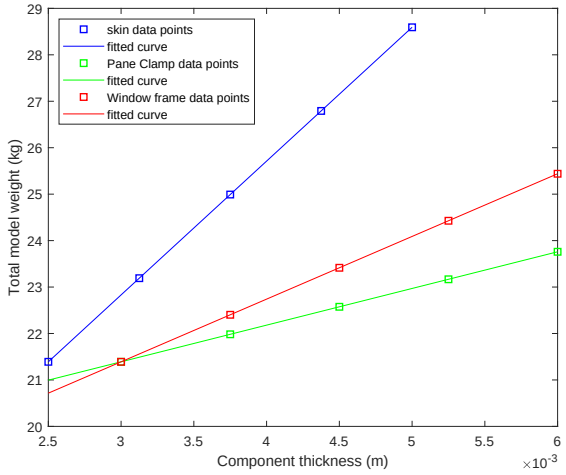

Figure 50: Total model weight sensitivity to Component thickness

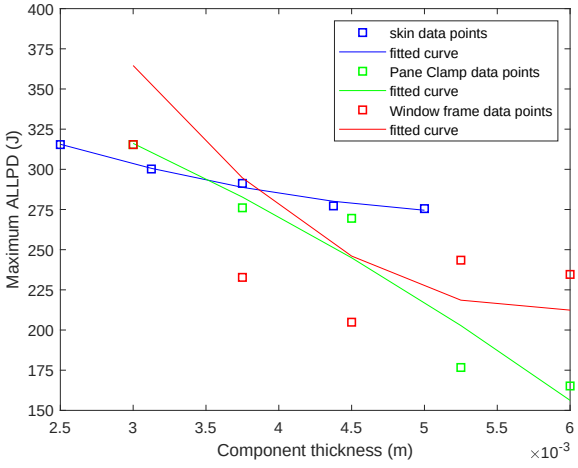

Figure 51: ALLPD sensitivity to Component thickness.

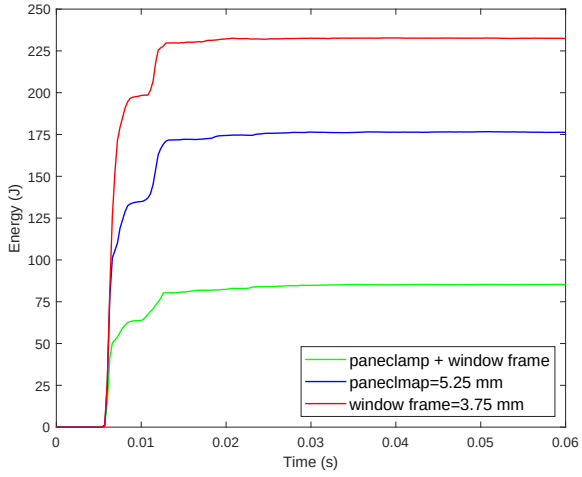

Figure 52: Combining the thickness of the pane clamp and the window frame can further decrease ALLPD compared to thickness increment of single components.

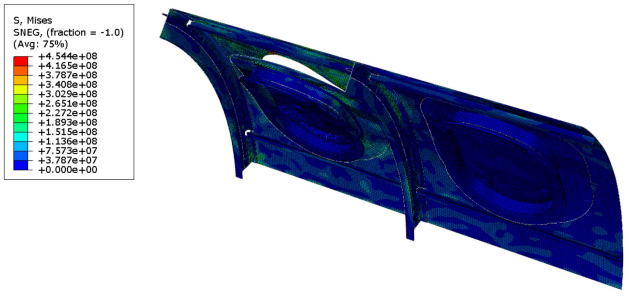

Figure 53: Passenger window penetration with a 133 m/s impact.